Cellular Context Dictates the Suppression or Augmentation of Triple-Negative Mammary Tumor Metastasis by NLRX1

Margaret A. Nagai-Singer,* Mackenzie K. Woolls,* Katerina Leedy,* Alissa Hendricks-Wenger,† Rebecca M. Brock,† Sheryl Coutermarsh-Ott,* Tamalika Paul,* Holly A. Morrison,* Khan M. Imran,† Juselyn D. Tupik,* Endia J. Fletcher,‡ David A. Brown,§ and Irving C. Allen*

Prior studies have defined multiple, but inconsistent, roles for the enigmatic pattern recognition receptor NLRX1 in regulating several cancer-associated biological functions. In this study, we explore the role of NLRX1 in the highly metastatic murine 4T1 mammary tumor model. We describe a functional dichotomy of NLRX1 between two different cellular contexts: expression in healthy host cells versus expression in the 4T1 tumor cells. Using *Nlrx1*$^{-/-}$ mice engrafted with 4T1 tumors, we demonstrate that NLRX1 functions as a tumor suppressor when expressed in the host cells. Specifically, NLRX1 in healthy host cells attenuates tumor growth and lung metastasis through suppressing characteristics of epithelial–mesenchymal transition and the lung metastatic niche. Conversely, we demonstrate that NLRX1 functions as a tumor promoter when expressed in 4T1 tumor cells using gain- and loss-of-function studies both in vitro and in vivo. Mechanistically, NLRX1 in the tumor cells augments 4T1 aggressiveness and metastasis through regulating epithelial–mesenchymal transition hallmarks, cell death, proliferation, migration, reactive oxygen species levels, and mitochondrial respiration. Collectively, we provide critical insight into NLRX1 function and establish a dichotomous role of NLRX1 in the 4T1 murine mammary carcinoma model that is dictated by cellular context. ***The Journal of Immunology*****, 2023, 211: 1844–1857.**

One in eight females will be diagnosed with breast cancer in their lifetime, making it one of the most prevalent and deadly malignancies in the United States (1, 2). Triple-negative breast cancer (TNBC), which is characterized by the absence of estrogen receptor (ER), progesterone receptor (PR), and HER2, is deadlier and more aggressive than other types of breast cancer (1, 2). Many biological pathways and processes that are important to the initiation and progression of cancers, including TNBC, are regulated in part through proteins associated with innate immune signaling such as pattern recognition receptors (PRRs). PRRs allow cells to sense pathogens, cellular damage, and stress and are often the first line of defense to microenvironmental changes in tissue homeostasis that are highly relevant to tumorigenesis and disease burden (3).

Specifically, PRRs recognize damage- and/or pathogen-associated molecular patterns to initiate or regulate the subsequent immune response, typically through the formation of multiprotein complexes. NOD-like receptors (NLRs) are a group of cytosolic PRRs that are best known for their ability to form a multiprotein complex known as the inflammasome, which initiates inflammation through production of IL-18 and IL-1β (4, 5). Although the inflammasome-forming NLRs are the best characterized, many NLR proteins do not directly participate in inflammasome formation and are classified as regulatory NLRs (6, 7). Most studies to date have focused on the role of these regulatory NLRs in inflammation, typically in the context of infectious diseases where they appear to regulate signaling associated with other PRRs and function through the formation of other multiprotein complexes such as the "NODosome" and the hypothesized "TRAFasome," but their mechanisms remain largely undefined (6–15).

NLRX1 is a unique and enigmatic regulatory NLR that functions to attenuate inflammation (16, 17). This has been best described in

*Department of Biomedical Sciences and Pathobiology, Virginia-Maryland College of Veterinary Medicine, Virginia Tech, Blacksburg, VA; †Graduate Program in Translational Biology, Medicine and Health, Virginia Tech, Roanoke, VA; ‡Postbaccalaureate Research Education Program, Virginia Tech, Blacksburg, VA; and §Stealth BioTherapeutics, Needham, MA

ORCIDs: 0000-0001-6687-6476 (M.A.N.-S.); 0000-0003-0957-728X (M.K.W.); 0000-0003-0433-3390 (K.L.); 0000-0001-8561-8288 (A.H.-W.); 0000-0003-4022-6189 (R.M.B.); 0000-0001-7385-3969 (S.C.-O.); 0000-0002-4888-5915 (T.P.); 0000-0001-7358-7728 (H.A.M.); 0000-0003-0755-8499 (K.M.I.); 0009-0003-8323-627X (E.J.F.); 0000-0001-5489-313X (D.A.B.); 0000-0001-9573-5250 (I.C.A.).

Received for publication November 9, 2022. Accepted for publication October 12, 2023.

This work was supported by the National Cancer Institute Grants R01CA269811 and R01CA274439 and by National Institute of Biomedical Imaging and Bioengineering Grant R01CA274439. The content is solely the responsibility of the authors and does not necessarily represent the official views of the National Institutes of Health. This work was also supported by the Virginia-Maryland College of Veterinary Medicine, the Virginia Tech Center for Engineered Health, the Institute for Critical Technologies and Applied Science, Virginia Tech, and the Virginia Tech Center for Drug Discovery.

Conceptualization, M.A.N.-S. and I.C.A.; methodology, M.A.N.-S. and I.C.A.; formal analysis, M.A.N.-S., S.C.-O., and D.A.B.; investigation, M.A.N.-S., M.K.W., K.L., A.H.-W., R.M.B., H.A.M., K.M.I., J.D.T., T.P., and E.J.F.; writing—original draft, M.A.N.-S.; writing—review and editing, M.A.N.-S., M.K.W., K.L., A.H.-W., R.M.B., S.C.-O., H.A.M., K.M.I., J.D.T., E.J.F., D.A.B., and I.C.A.; visualization, M.A.N.-S.; supervision, I.C.A.; project administration, I.C.A.; funding acquisition, I.C.A.

The microarray data presented in this article have been submitted to the Gene Expression Omnibus (https://www.ncbi.nlm.nih.gov/geo/query/acc.cgi?acc=GSE216937) under accession number GSE216937.

Address correspondence and reprint requests to Dr. Irving C. Allen, Virginia Tech, College of Veterinary Medicine, IDRF 140, 295 Duckpond Drive, Blacksburg, VA 24061. E-mail address: icallen@vt.edu

The online version of this article contains supplemental material.

Abbreviations used in this article: DEG, differentially expressed gene; EMT, epithelial–mesenchymal transition; ER, estrogen receptor; NLR, NOD-like receptor; ORF, open reading frame; PR, progesterone receptor; PRR, pattern recognition receptor; ROS, reactive oxygen species; shRNA, short hairpin RNA; TAC, Transcriptome Analysis Console; 4T1^{KD}, 4T1 knockdown; 4T1$^{KD\text{-}CTL}$, 4T1^{KD} control; TNBC, triple-negative breast cancer; 4T1^{OE}, 4T1 overexpression; 4T1$^{OE\text{-}CTL}$, 4T1^{OE} control; WT, wild-type.

https://doi.org/10.4049/jimmunol.2200834

the context of host–pathogen immune signaling, where NLRX1 attenuates proinflammatory NF-κB signaling and inhibits the interaction between RIG-I and MAVS to attenuate type I IFN (8, 10, 11, 18, 19). Additionally, NLRX1 regulates other major signaling pathways that involve STAT, MAPK, JNK, and AKT signaling, albeit through mechanisms that are not entirely defined (20–26). NLRX1 can also modulate reactive oxygen species (ROS) production, autophagy, and metabolism under specific biological conditions that are not fully understood (25–38). The regulation of these numerous and diverse pathways by NLRX1 suggests that NLRX1 can contribute to a wide range of human diseases, including cancer (7, 16, 17).

The role of NLRX1 in several cancer models has proven to be enigmatic due in large part to conflicting data between different types and subtypes of cancer. For example, NLRX1 has been suggested to function as a tumor suppressor in models of colon cancer, including spontaneous and azoxymethane/dextran sodium sulfate mouse models and human colon cancer cells engrafted into mice (20, 24, 27). NLRX1 also appears to protect against disease burden in histiocytic sarcoma and hepatocellular carcinoma models (21, 23). Many of these phenotypes seem to be driven by its modulation of pathways including ERK, STAT3, NF-κB, MAPK, and AKT signaling. Conversely, conflicting data have been reported that demonstrate NLRX1 functions as a tumor promoter in some situations, such as azoxymethane-only models of colorectal cancer (non-inflammation driven) and human papillomavirus–associated head and neck squamous cell carcinoma (37, 38). These studies illustrate that genetic modification of NLRX1 results in robust phenotypes in all cancer models reported, but the tumor-suppressing or tumor-promoting role of NLRX1 is complex and nuanced.

The complexity of NLRX1 function extends to breast cancer, where its role remains controversial and apparently dependent on the aggressiveness and type of breast cancer cell. For example, NLRX1 is upregulated in aggressive TNBC cell lines compared with less aggressive ER/PR-positive cell lines (27, 36). Likewise, in human tumors, NLRX1 is upregulated in TNBC tumors and metastatic tumors compared with ER/PR-positive tumors and early-stage tumors (36). In vitro, NLRX1 overexpression in MCF-7 human breast cancer cells (ER/PR-positive) demonstrated decreased clonogenicity and migration and suggested that NLRX1 is tumor-suppressing (27). Conversely, NLRX1 knockdown in MDA-MB-231 human TNBC cells (ER/PR-negative) demonstrated decreased proliferation and migration and suggested that NLRX1 is tumor-promoting (36). Taken together, these previous studies have shown a role for NLRX1 in regulating biological functions during breast cancer. However, these studies lacked in vivo model assessments and did not conduct loss- and gain-of-function studies in consistent cell lines, which limited the exploration of NLRX1 and restricted more comprehensive mechanistic studies.

To address these issues, we generated novel *Nlrx1*$^{-/-}$ mice on the BALB/cJ background, which is the strain required for the commonly used 4T1 murine triple-negative mammary tumor model. We also generated 4T1 cell lines to conduct critical loss-of-function and gain-of-function studies within the same parental cell line both in vitro and in vivo. In this study, using these unique mice and cell lines, we show that the biological effects of NLRX1 in murine mammary tumors are highly dependent on the cellular context (healthy host cells versus tumor cells). Using *Nlrx1*$^{-/-}$ mice, we show that NLRX1 functions as a tumor suppressor in healthy host cells, where it protects against tumor progression and metastasis through regulating epithelial–mesenchymal transition (EMT) markers, recruitment of immune cells, and the formation of the lung metastatic niche. Conversely, in the 4T1 tumor cells, NLRX1 augments tumor progression and metastasis by increasing malignant properties in vitro and promoting EMT characteristics and disease burden in vivo. Taken together, by using combined in vitro and in vivo models that can be evaluated together and in parallel, our data demonstrate a functional dichotomy between NLRX1 in healthy host cells versus in mammary tumor cells, especially regarding mammary tumor metastasis.

Materials and Methods

Cell culture and transfection

4T1 cells were obtained from American Type Culture Collection and were cultured in RPMI 1640 (American Type Culture Collection) supplemented with 10% FBS (R&D Systems) and 1% penicillin/streptomycin (Thermo Fisher Scientific). Cells were incubated at 37°C and 5% CO_2. 4T1 cells were transduced to either knock down (4T1^{KD}) murine NLRX1 using lentiviral short hairpin RNA (shRNA) particles or overexpress (4T1^{OE}) murine NLRX1 using lentiviral open reading frame (ORF) particles, according to the manufacturer's protocols (Origene TL515304V and MR213673L4V). Knockdown control 4T1 cells (4T1$^{KD\text{-}CTL}$) were transduced with scrambled shRNA particles, and overexpression control 4T1 cells (4T1$^{OE\text{-}CTL}$) were transduced with control ORF particles (Origene TR30021V and PS100093V). Antibiotic selection with 3 μg/ml puromycin (Santa Cruz Biotechnology) was used to select for transduced cells, and successful overexpression or knockdown was confirmed by Western blot for murine NLRX1 (Abcam). Four different shRNA sequences were tested for generating the 4T1^{KD} cells, and one sequence proved to be superior during puromycin selection. Cells were authenticated using morphology checks by microscope and commercial *Mycoplasma* testing (Charles River Research Animal Diagnostic Services) and were discarded before 30 passages. Importantly, due to differences in the shRNA technology used for the knockdown system (4T1^{KD} and 4T1$^{KD\text{-}CTL}$) versus the ORF technology used for overexpression system (4T1^{OE} and 4T1$^{OE\text{-}CTL}$), each transduced cell line was only compared with its specific internal control.

Cell migration assay

Transduced 4T1 cells were seeded at 5×10^5 cells per well in a six-well plate in complete media and incubated overnight. Media were then switched to 1% FBS media and incubated for 24 h to allow cells to adjust to the decreased serum content. A 200-μl pipette tip was used to make three scratches per well for a "scratch" assay. Initial images of each scratch were acquired directly following the scratch induction (Invitrogen EVOS M5000). At 5 and 8 h postscratch, images of each scratch were acquired at the same location of the initial image. Images were uploaded to Fiji/ImageJ, and the width of the scratch was measured several times per image. Rate of migration was calculated as pixels per hour.

Proliferation assay

Transduced 4T1 cells were seeded at 1×10^4 cells per well in a 96-well plate in complete media and incubated overnight. Media were then replaced with experimental media of complete media with and without 10 ng/ml TNF (PeproTech), and with and without 10 ng/ml TGF-β (R&D Systems) and allowed to incubate for 48 h. An MTT assay was performed according to the manufacturer's protocols (Abcam).

Cell death assay

Transduced 4T1 cells were seeded at 1×10^4 cells per well in a 96-well plate in complete media and incubated overnight. Media were then replaced with complete media with and without 100 mM H_2O_2 (Fisher Chemical) and allowed to incubate for 6 h. A lactate dehydrogenase assay was performed according to manufacturer's protocols (Thermo Fisher Scientific).

Mitochondrial ROS production

Transduced 4T1 cells were seeded at 1×10^5 cells per well in a 24-well plate in complete media and incubated overnight. Media were then replaced with complete media with and without 10 ng/ml TNF (PeproTech) and incubated for 4 h. MitoSOX (Thermo Fisher Scientific) and NucBlue (Thermo Fisher Scientific) were added to the wells per the manufacturer's protocols. Several images per well were acquired with a fluorescent microscope (Invitrogen EVOS M5000). Fluorescence intensity of each image was measured using Fiji/ImageJ and corrected for background fluorescence in unstained samples.

Metabolism assays

Transduced 4T1 cells were seeded at 1×10^4 cells per well in a 96-well Seahorse XF96 cell culture microplate (Agilent) in complete media and allowed to attach for 3 h. Media were then replaced with experimental media of

complete media with and without 10 ng/ml TNF (PeproTech) and with and without 10 ng/ml TGF-β (R&D Systems) and incubated for 24 h. A Seahorse XF96 Mito Stress Test (Agilent) was performed according to the manufacturer's protocols at the Virginia Tech Metabolism Core. Respiratory capacity was calculated as maximal respiration minus basal respiration of the final time point of each injection step and corrected for nonmitochondrial respiration.

Western blotting

Protein was extracted from cells or tissues in a protein lysis buffer of 2% SDS, 100 mM Tris HCl, 100 mM NaCl, and 1× protease inhibitor (Thermo Fisher Scientific) and quantified using a bicinchoninic acid assay (Thermo Fisher Scientific) according to the manufacturer's protocols. Samples were loaded at 20 μg/ml with reducing sample buffer (Thermo Fisher Scientific) in precast 4–12% Bis-Tris mini protein gels (Thermo Fisher Scientific), transferred to a polyvinylidene difluoride membrane in 1× TGE (Tris-glycine-EDTA) + 20% methanol, and blocked in 5% milk in TBS + 0.1% Tween 20 (TBST). All Abs were diluted 1:1000 in 5% BSA or 5% milk and incubated overnight at 4°C (CST and Abcam). TBST was used for all wash steps. Images were obtained with iBright (Thermo Fisher Scientific) or Odyssey XF (LI-COR Biosciences) imaging systems using an HRP-conjugated secondary Ab (CST) and SuperSignal West Pico, Dura, or Femto Chemiluminescent Substrates (Thermo Fisher Scientific). In all Western blots performed on tissue samples, each lane represents an individual mouse and therefore represents natural variabilities between individual mice.

Flow cytometry

Tumors and lungs were collected in cold RPMI 1640 and mechanically and/or enzymatically digested as previously described (39). Cells were counted with trypan blue and diluted to 1×10^7 cells/ml. Then, 100 μl of each sample was collected in a microcentrifuge tube and fixed with a formaldehyde-based fixation buffer (Invitrogen) for 15 min in the dark. Fixed cells were resuspended in PBS and stored at 4°C in the dark until staining. Permeabilization was conducted on samples in panel 2 using a permeabilization buffer for 20 min at room temperature in the dark (Invitrogen). Staining was conducted with Abs diluted in FACS buffer following blocking with an Fc-blocking Ab and samples were submitted to the Flow Cytometry Core at Virginia Tech, who also performed the gating. The flow cytometry panels and sample gating for the population that includes potential eosinophils can be found in Supplemental Fig. 1.

Generation of BALB/cJ Nlrx1$^{-/-}$ *mice*

BALB/cJ *Nlrx1*$^{-/-}$ mice were generated through 12 generations of backcrossing. C57/BL6J *Nlrx1*$^{-/-}$ mice (provided by Dr. Jenny Ting, University of North Carolina at Chapel Hill) were crossed with wild-type (WT) BALB/cJ mice purchased from The Jackson Laboratory to create *Nlrx1*$^{+/-}$ offspring (10). Each generation of *Nlrx1*$^{+/-}$ offspring was crossed with WT BALB/cJ mice for 12 generations. F_{12} *Nlrx1*$^{+/-}$ mice were crossed with each other to generate the first BALB/cJ *Nlrx1*$^{-/-}$ offspring, which established the colony of BALB/cJ *Nlrx1*$^{-/-}$ mice. WT and *Nlrx1*$^{-/-}$ mice were maintained as separate colonies. All mice were housed under specific pathogen-free conditions, and all experiments were conducted under the approval of the Virginia Tech Institutional Animal Care and Use Committee and the National Institutes of Health *Guide for the Care and Use of Laboratory Animals*.

Genotyping

We confirmed the genotype of all mice generated from backcrossing. Tail snips were collected for DNA extraction. DNA extraction was performed using 25 mM NaOH/0.2 mM EDTA and 40 mM Tris-HCl. MyTaq (Bioline) and three *Nlrx1* primers (5′-CCAGGCTCAGCATAATTTGTT-3′, 5′-AGCCGGAAGTCAAGGTTGAGG-3′, and 5′-AGCGCATCGCCTTCTATCGCCTTC-3′) were used for PCR. PCR product was loaded into a 2% LE (low electroendosmosis) agarose gel with ethidium bromide and set to run for 60 min at 150 V. Gel images were obtained with iBright (Thermo Fisher Scientific) or Odyssey XF (LI-COR Biosciences) imaging systems.

In vivo 4T1 models

Experimental mice were all females between 2 and 5 mo of age. Mice were anesthetized and injected with 1.2×10^6 4T1 cells (4T1, 4T1^{OE}, 4T1$^{OE\text{-}CTL}$, 4T1^{KD}, or 4T1$^{KD\text{-}CTL}$) in 100 μl of sterile PBS in the left abdominal mammary fat pad (39). An estimation of tumor volume was calculated as (length × width × width)/2. Morbidity was determined through scoring activity level, respiration, movement, appearance, and tumor condition on a scale of 0 (normal) to 4 (severe complications). Tumors were collected for final tumor volume, calculated as (3.14159/6) × length × width × height as previously described (40). Sections of the tumors were fixed in 10% formalin for H&E analysis, flash-frozen for RNA/protein extraction, or harvested for flow cytometry. Lungs were collected for metastasis quantification as previously described, with quantification done either by manually counting 6-thioguanine–resistant metastatic colonies ("metastatic colonies") or by using computer-based imaging to calculate the percentage of positive staining for 6-thioguanine–resistant metastatic colonies ("% metastatic burden") (39, 41). Lungs were also flash-frozen for RNA/protein extraction or harvested for flow cytometry. Whole blood was collected for metastasis quantification as previously described (41). All experiments were conducted with Institutional Animal Care and Use Committee approval and in accordance with the National Institutes of Health *Guide for the Care and Use of Laboratory Animals*.

Gene expression and transcriptomics

RNA was extracted from flash-frozen tumors using a RNeasy isolation kit per the manufacturer's protocols (Qiagen). For the pathway-focused quantitative RT-PCR array, total RNA from three 4T1 tumors was pooled per genotype (WT and *Nlrx1*$^{-/-}$). Gene expression was evaluated with a murine breast cancer RT^2 Profiler PCR array (Qiagen). Ingenuity Pathway Analysis was used to predict pathways impacted by differentially expressed genes (DEGs). For transcriptomics analysis, RNA from three to six tumors were divided and pooled into two separate replicates for 4T1, 4T1^{OE}, or 4T1$^{OE\text{-}CTL}$ tumors from each genotype (WT and *Nlrx1*$^{-/-}$), for a total of six groups with two replicates each. Gene expression was evaluated using microarray analysis (Clariom S, Applied Biosystems, Thermo Fisher Scientific). Data were analyzed using Transcriptome Analysis Console (TAC) (Applied Biosystems, Thermo Fisher Scientific). TAC predicts the real-life significance of a gene/pathway through analyzing multiple parameters and is not to be confused with statistical significance. A combination of TAC and Ingenuity Pathway Analysis data were used to inform the working models presented in this manuscript.

Statistical analysis

Animal numbers were justified by a power analysis. Comparisons were analyzed using a two-way unpaired *t* test or an ANOVA followed by a Tukey post hoc test for multiple comparisons as appropriate. Survival was analyzed using a log-rank Mantel–Cox test. All figures and analyses were completed in GraphPad Prism. Outlier tests were conducted to identify and remove any outliers in the data when appropriate.

Data availability

Microarray data presented in this study are publicly available at Gene Expression Omnibus under accession number GSE216937 (https://www.ncbi.nlm.nih.gov/geo/query/acc.cgi?acc=GSE216937).

Results

NLRX1 expressed in healthy host cells attenuates tumor progression and metastasis

To determine the role of NLRX1 in healthy host cells on mammary tumor progression, we generated novel BALB/cJ *Nlrx1*$^{-/-}$ mice compatible with the 4T1 triple-negative mammary tumor model. These mice were generated through 12 generations of backcrossing and were confirmed to lack a functional *Nlrx1* gene. *Nlrx1*$^{-/-}$ and WT BALB/cJ mice were injected with 1.2×10^6 4T1 cells in a single mammary fat pad and were monitored for tumor growth, morbidity, and mortality. During the course of the study, *Nlrx1*$^{-/-}$ mice increasingly presented with larger tumors than WT mice did (Fig. 1A), and no differences in morbidity (Fig. 1B) or mortality (Fig. 1C) were observed. However, because tumor measurements throughout the study only accounted for the length and width of the tumor, we calculated the final tumor volume of excised tumors to include tumor depth. This three-dimensional measurement confirmed that *Nlrx1*$^{-/-}$ mice developed larger tumors than WT mice do (Fig. 1D). *Nlrx1*$^{-/-}$ mice also exhibited an increase in metastatic burden in the lung compared with WT animals (Fig. 1E, 1F). *Nlrx1*$^{-/-}$ mice had ~6-fold more circulating tumor cells in the blood than WT animals did; however, this assessment was highly variable and results were not statistically significant ($p = 0.2$) (Fig. 1G). Taken together, the increased tumor volume and metastasis in *Nlrx1*$^{-/-}$ mice demonstrate that NLRX1 attenuates 4T1 tumor progression when expressed by host cells.

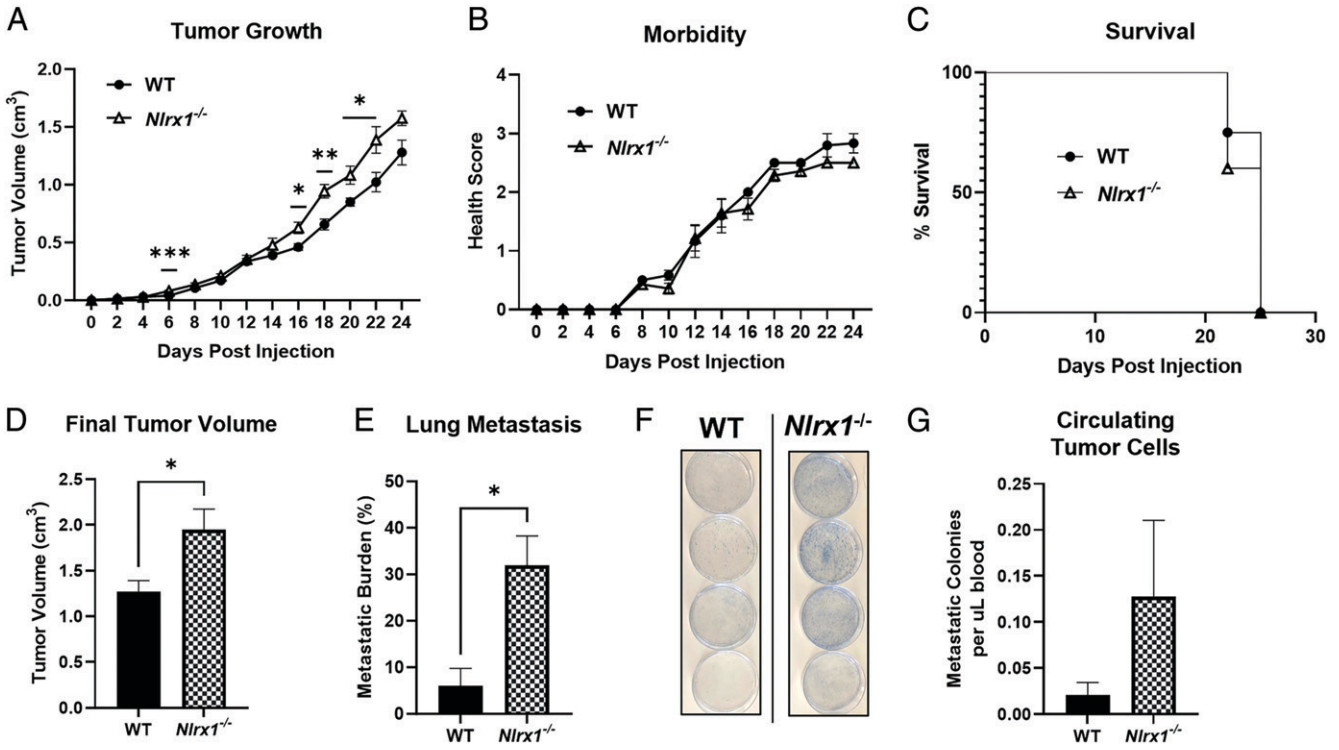

FIGURE 1. NLRX1 expressed in healthy host cells attenuates tumor progression and metastasis. (**A**) Tumor volume estimate based on two-dimensional measurements. (**B**) Morbidity and (**C**) mortality were not significantly impacted by mouse genotype. (**D**) Three-dimensional final tumor volume measurements. (**E** and **F**) Differences between WT and *Nlrx1*$^{-/-}$ mice in (E) quantification of lung metastasis and (F) representative images of lung metastatic colonies. (**G**) Quantification of circulating tumor cells in the blood. Lung metastasis, circulating tumor cells, and final tumor volume were analyzed using a two-way unpaired *t* test. Tumor growth and morbidity were analyzed using multiple *t* tests (one per row). Survival was analyzed using a log-rank Mantel–Cox test. WT, $n = 5$; *Nlrx1*$^{-/-}$, $n = 7$. Data are representative of two independent experiments. All data are displayed as mean ± SEM. *$p \leq 0.05$, **$p \leq 0.01$, ***$p \leq 0.001$.

LRX1 expressed in host cells decreases metastasis by limiting EMT characteristics and immune cell recruitment

To begin uncovering the mechanisms responsible for this protective phenotype, we next profiled gene expression in 4T1 tumors collected from WT and *Nlrx1*$^{-/-}$ mice using both whole-transcriptome microarrays and pathway-focused quantitative RT-PCR arrays. The transcriptome analysis identified the top 20 pathways that were altered in tumors from *Nlrx1*$^{-/-}$ mice versus tumors from WT animals based on the number of DEGs (Fig. 2A). This revealed many pathways associated with the prometastatic process of EMT (Fig. 2A). Specifically, in the absence of NLRX1, several genes associated with EGFR1 signaling, focal adhesion, PI3K-AKT-mTOR, c-Kit receptor signaling, and TGF-β receptor signaling were upregulated compared with tumors from WT mice, indicating that NLRX1 may regulate EMT (Fig. 2B). Indeed, we identified 12 DEGs highly relevant to EMT, suggesting that NLRX1 attenuates EMT gene signatures in the host cells (Fig. 2C, Supplemental Fig. 2A) (42). To validate that NLRX1 regulates EMT, we analyzed protein levels of the epithelial marker E-cadherin, which is commonly found to be downregulated in cells undergoing EMT (43). The Western blot data revealed that tumors from *Nlrx1*$^{-/-}$ mice express approximately half the E-cadherin of tumors from WT mice (Fig. 2D, Supplemental Fig. 2B). We also analyzed protein levels of TGF-β and MMP9, both of which promote EMT (44). We found that more tumors from *Nlrx1*$^{-/-}$ mice express MMP9 and TGF-β compared with tumors from WT mice (Fig. 2E, Supplemental Fig. 2B). This further suggests a protective role for NLRX1 against EMT when expressed by healthy host cells. Using Ingenuity Pathway Analysis of the targeted RT-PCR array data and the TAC analysis of the transcriptomics data, the analyses predicted specific interactions resulting in the phenotypes observed in the *Nlrx1*$^{-/-}$ mice (Fig. 2F, Supplemental Fig. 2C, 2D). The results predict that NLRX1 limits EMT by suppressing TGF-β, c-Kit, and EGF signaling, which further suppresses the downstream activation of the PI3K-AKT, ERK1/2, and β-catenin pathways. These pathways appear to converge on the pro-EMT transcription factor *Zeb2* (Fig. 2F). Ultimately, the loss of NLRX1 in healthy host cells facilitates the emergence of EMT hallmarks, which in turn may facilitate the increased metastasis in *Nlrx1*$^{-/-}$ animals.

Immune cells provide a critical niche that can facilitate tumor progression, invasion, and metastasis through modulating EMT (45, 46). Thus, we next sought to define the tumor microenvironment of the tumors from WT and *Nlrx1*$^{-/-}$ mice using flow cytometry. Using a well-defined panel of cell surface markers (Supplemental Fig. 1A), most leukocyte populations evaluated did not have any statistical differences (Supplemental Fig. 2E). However, intriguingly, tumors from *Nlrx1*$^{-/-}$ mice contained significantly more cells resembling eosinophils than tumors from WT animals did (Fig. 2G, 2H). Importantly, although this population would include eosinophils, the generalness of the cell surface markers used in this study cannot confirm that this population includes only eosinophils. We refer to this population as "eosinophil-containing" to indicate the uncertainty of the exact makeup of this population. Eosinophils can drive EMT through the secretion of MMP9 and TGF-β, which as noted above were observed in more tumors from *Nlrx1*$^{-/-}$ mice (Fig. 2E) (47). The increased eosinophil-containing population appears to be correlated with a significant decrease in *Cxcl9* observed in the *Nlrx1*$^{-/-}$ tumors (Fig. 2I). CXCL9 inhibits eosinophil recruitment and has previously been shown to be dysregulated in the absence of

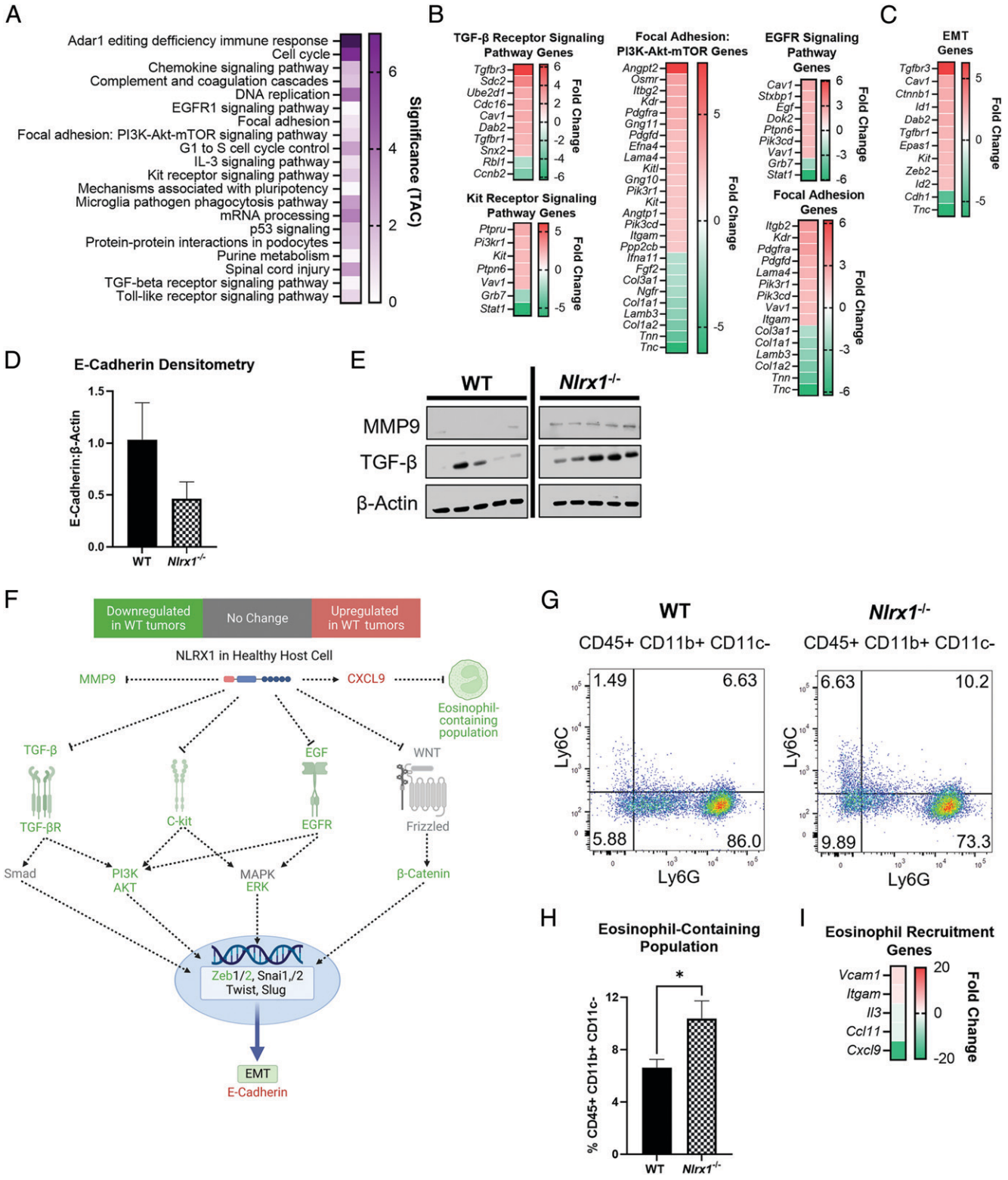

FIGURE 2. NLRX1 expressed in healthy host cells decreases metastasis by limiting epithelial–mesenchymal transition characteristics and immune cell recruitment. (**A**) Transcriptomics assessments identified the top 20 pathways altered in tumors harvested from *Nlrx1*$^{-/-}$ versus WT mice, defined by the number of DEGs in the Transcriptomics Analysis Console (TAC) software. Pathways are listed alphabetically as a heat map by TAC significance (*Nlrx1*$^{-/-}$ tumors versus WT tumors). (**B**) Heat maps of the DEGs from epithelial–mesenchymal transition (EMT)–related pathways in TAC (*Nlrx1*$^{-/-}$ tumors versus WT tumors). (**C**) Heat map of DEGs from EMT-related genes (*Nlrx1*$^{-/-}$ tumors versus WT tumors). (**D** and **E**) Differences in (D) densitometry of E-cadherin and (E) protein levels of MMP9 and TGF-β. (**F**) Ingenuity Pathway Analysis and TAC analysis were used to generate a model of EMT-related pathways altered by NLRX1. (**G** and **H**) Differences in the eosinophil-containing population shown as (G) representative scatter plots and (H) quantification of flow cytometry data. WT, $n = 5$; *Nlrx1*$^{-/-}$ tumors, $n = 5$. Data were analyzed using two-way unpaired t test and shown as mean ± SEM. See also Supplemental Fig. 2. *$p \leq 0.05$. (**I**) Heat map of five DEGs (*Nlrx1*$^{-/-}$ tumors versus WT tumors) associated with eosinophil recruitment.

NLRX1 in other models (38, 48, 49). However, the mechanisms associated with the NLRX1–CXCL9 regulation remain undefined and speculative (38, 49, 50). Taken together, our data in the *Nlrx1*$^{-/-}$ mice provide a working model in which NLRX1 attenuates tumor progression and metastasis through the upregulation of CXCL9, which limits the recruitment of pro-EMT eosinophil-containing populations and the subsequent production of MMP9 and TGF-β to suppress EMT.

NLRX1 expressed in healthy host cells attenuates lung metastasis through limiting the formation of the metastatic niche

The priming of distant organs to create favorable environments for metastatic seeding allows tumor cells that have undergone EMT to find a hospitable location beyond the primary tumor (51). NLRX1 has been implicated in several hallmarks of this metastatic niche, including inflammation, angiogenesis, immune suppression, and ECM remodeling (16, 17, 21, 52). Interestingly, there is also evidence of crosstalk between the metastatic niche and tumor cells undergoing EMT (53). Thus, due to the increased lung metastasis and EMT characteristics in the *Nlrx1*$^{-/-}$ mice, we next sought to determine whether NLRX1 impacts the metastatic niche in the lung.

In the 4T1 model, tumor cells consistently become metastatic by day 8 postinjection (39). To evaluate the evolution of the metastatic niche in WT and *Nlrx1*$^{-/-}$ mice, we conducted assessments throughout 4T1 disease progression using Western blot analysis at premetastasis (day 7) and postmetastasis (day 14) time points. At the premetastatic time point, lungs from *Nlrx1*$^{-/-}$ mice contained increased levels of MMP9 and TGF-β compared with lungs from WT animals. Lox, fibronectin, and IL-6 were expressed in more *Nlrx1*$^{-/-}$ lungs compared with WT lungs (75 versus 50%, 75 versus 50%, and 50 versus 25% of lungs sampled, respectively) (Fig. 3A, Supplemental Fig. 3A). Increased levels of these proteins have been correlated with increased metastasis in various cancer models and are commonly used to define the metastatic niche (54). These data suggest that NLRX1 attenuates premetastatic niche formation through ECM remodeling and suppressing inflammation in the lung. At the postmetastasis time point, lungs from *Nlrx1*$^{-/-}$ mice demonstrated increased levels of MMP9 and IL-6. However, postmetastatic lungs from *Nlrx1*$^{-/-}$ mice lost the premetastatic increases in TGF-β, and they reversed the percentage of tumors expressing fibronectin (0 versus 60%) and Lox (20 versus 40%) (Fig. 3B, Supplemental Fig. 3B). These data suggest that the lung metastatic niche shifts as the tumor cells begin to colonize the organ, but that NLRX1 still suppresses characteristics of the metastatic niche after metastasis has begun.

To define how NLRX1 impacts the immune cells involved in metastatic niche formation, we also evaluated immune cell populations in the lungs at the pre- and postmetastasis time points. There were no significant differences in most leukocyte populations at the premetastasis time point (Supplemental Fig. 3C). However, lungs from *Nlrx1*$^{-/-}$ mice had significantly more inflammatory dendritic cells and NK cells compared with WT lungs (Fig. 3C, 3D, Supplemental Fig. 3D, 3E). The increase in inflammatory dendritic cells in *Nlrx1*$^{-/-}$ lungs suggests an increase in inflammation in *Nlrx1*$^{-/-}$ mice, which is consistent with our Western blot data. Additionally, although the accumulation of NK cells in *Nlrx1*$^{-/-}$ lungs might appear counterintuitive to our phenotype, previous literature has identified an influx of NK cells that lack effector functions to the lung metastatic niche, which would be consistent with our observations (53). At the postmetastasis time point, there were no significant differences in any of the immune cell populations evaluated (Supplemental Fig. 3F). These data indicate the loss of NLRX1 in the lung creates an environment that is consistent with hallmarks of the premetastatic niche and therefore may facilitate the increased lung metastasis in *Nlrx1*$^{-/-}$ mice we observed in vivo.

NLRX1 expressed in 4T1 cells enhances their aggressive properties in vitro

The experiments above in *Nlrx1*$^{-/-}$ mice establish that NLRX1 functions as a tumor suppressor when expressed systemically in the

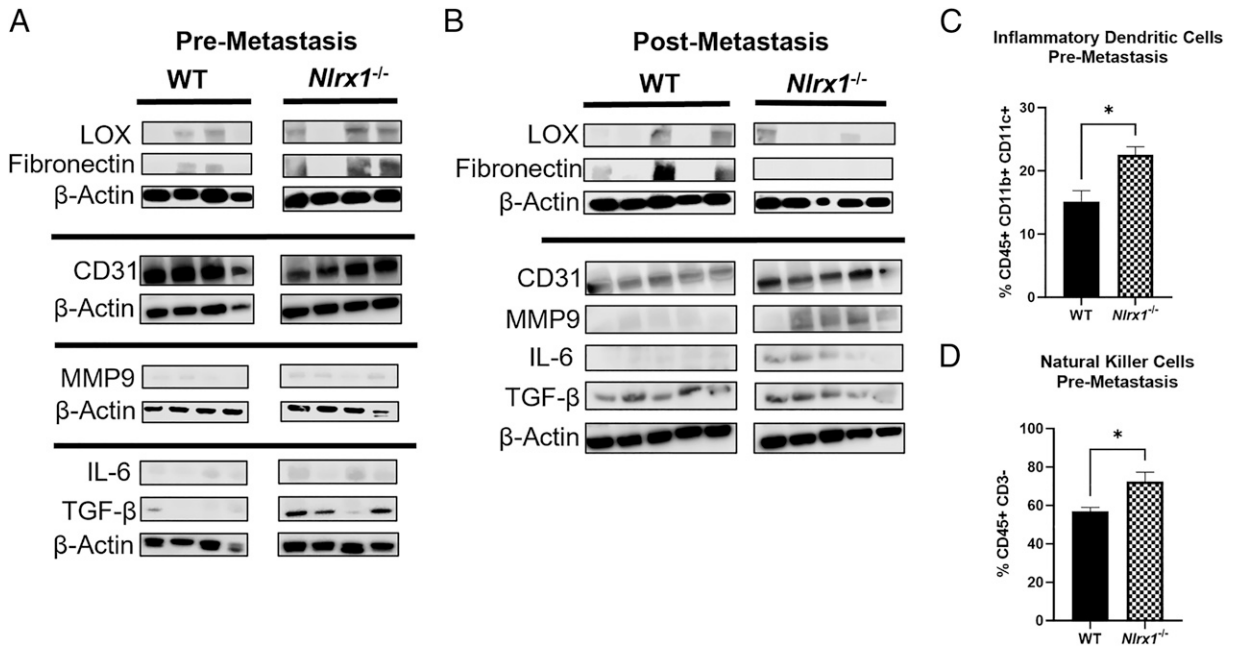

FIGURE 3. NLRX1 expressed in healthy host cells attenuates lung metastasis through limiting the formation of the metastatic niche. (**A** and **B**) Western blot analysis of MMP9, IL-6, TGF-β, LOX, fibronectin, and CD31 in (A) premetastasis lungs ($n = 4$ per genotype) and (B) postmetastasis lungs ($n = 5$ per genotype). (**C** and **D**) Quantification of (C) inflammatory dendritic cells and (D) NK cells in premetastasis lungs evaluated using flow cytometry ($n = 4$ per genotype). Western blot images are representative of two experiments, and flow cytometry experiments were performed once. See also Supplemental Fig. 3. All quantification data were analyzed using a two-way unpaired *t* test and shown as mean ± SEM. *$p \leq 0.05$.

host. We next sought to determine the function of NLRX1 in the 4T1 mammary tumor cells through gain-of-function and loss-of-function studies. In this study, we used a stable lentiviral transduction to generate 4T1 cells that either overexpress ($4T1^{OE}$) or knock down ($4T1^{KD}$) NLRX1, as well as their respective controls ($4T1^{OE\text{-}CTL}$ and $4T1^{KD\text{-}CTL}$) (Fig. 4A). Importantly, NLRX1 is ubiquitously expressed and is typically expressed in mammary tissue (55, 56). Also of importance, due to the different technologies used for the overexpression system (ORF) versus knockdown systems (shRNA), $4T1^{OE}$ and $4T1^{KD}$ cells are not directly compared with each other. Instead, they are only compared with their internal controls ($4T1^{OE}$ versus $4T1^{OE\text{-}CTL}$, and $4T1^{KD}$ versus $4T1^{KD\text{-}CTL}$). Previous studies examining NLRX1 in breast cancer demonstrated opposing regulation of proliferation and cell death in different cell lines, so we sought to evaluate these processes in our model using MTT and lactate dehydrogenase assays (27, 36). $4T1^{OE}$ cells trended toward an increase in proliferation compared with $4T1^{OE\text{-}CTL}$ cells ($p = 0.08$). Conversely, $4T1^{KD}$ cells displayed decreased proliferation compared with $4T1^{KD\text{-}CTL}$ cells, with the knockdown cells undergoing proliferation at half of their control levels (Fig. 4B). We repeated this experiment using TNF to stimulate NLRX1 function as previously described or TGF-β to stimulate EMT (27, 36). Under these conditions, we observed no differences in the $4T1^{OE}$ cells but did continue to observe significantly decreased proliferation in the $4T1^{KD}$ cells (Fig. 4C, 4D). Cell death was evaluated following treatment with H_2O_2, where NLRX1 overexpression protected the 4T1 cells from H_2O_2-induced cell death, as shown by the decrease in cytotoxicity for the $4T1^{OE}$ cells compared with the $4T1^{OE\text{-}CTL}$ cells (Fig. 4E). Conversely, cells lacking NLRX1 were more sensitive to H_2O_2-induced cell death, as evidenced by the increase in cytotoxicity observed in $4T1^{KD}$ cells compared with $4T1^{KD\text{-}CTL}$ cells (Fig. 4E). Taken together, these data indicate that NLRX1 functions as a tumor promoter in 4T1 cells by attenuating ROS-mediated cell death and impacting proliferation.

Due to the metastasis phenotype observed in vivo, we next evaluated 4T1 migration potential using a common scratch assay. Previous literature has demonstrated differing scratch assay results based on the breast cancer cell line used (27, 36). At 5 and 8 h postscratch, NLRX1 overexpression in the $4T1^{OE}$ cells resulted in faster rates of migration compared with $4T1^{OE\text{-}CTL}$ cells, migrating approximately three times faster at each time point (Fig. 4F, 4G). Conversely, the loss of NLRX1 in the $4T1^{KD}$ cells reduced migration by ~40 and 50% compared with $4T1^{KD\text{-}CTL}$ cells at the 5- and 8-h time points, respectively (Fig. 4F, 4G). These data suggest that in addition to regulating proliferation and cell death, NLRX1 expression in the 4T1 tumor cells also increases their migration potential. In general, our 4T1 results thus far are consistent with data from MDA-MB-231 cells and are in contrast to data from MCF-7 cells (27, 36).

NLRX1 was originally characterized as being associated with the mitochondria in the context of infectious diseases, although its exact impact on mitochondrial function, including ROS production, continues to be an active area of research and debate (11, 16, 25–28, 34, 36, 57–59). Tumor cells routinely demonstrate increased ROS production and dysregulated mitochondrial dynamics, both of which can impact the survival and metastatic potential (60). Thus, we next sought to evaluate the role of NLRX1 in these biological functions in our transduced 4T1 cell lines. To evaluate superoxide levels, we used MitoSOX staining. Overexpression of NLRX1 in the $4T1^{OE}$ cells resulted in a significant increase in mitochondrial superoxide that was almost 6-fold ($\log_2$) higher than for the $4T1^{OE\text{-}CTL}$ control cells (Fig. 4H). Conversely, the loss of NLRX1 in the $4T1^{KD}$ cells resulted in a significant repression of mitochondrial superoxide, observed to be ~4-fold ($\log_2$) lower than their controls (Fig. 4H). We also observed that superoxide levels in $4T1^{KD\text{-}CTL}$ cells were similar to the $4T1^{OE}$ cells, rather than the $4T1^{OE\text{-}CTL}$ cells. We believe this reflects the differences in the transduction technologies used to knock down and overexpress *Nlrx1* (ORF versus shRNA) and confirms our rationale for comparing each modified cell line with its internal control. The regulation of ROS levels was retained following TNF stimulation in the knockdown system, but not the overexpression system (Fig. 4I). These findings are consistent with earlier studies in MCF-7 cells that showed overexpression of NLRX1 promotes ROS production, but they are in contrast to ROS production data previously published for MDA-MB-231 cells (27, 36).

To better define the role of NLRX1 in mitochondria function and energetics, we used a Seahorse XF Mito Stress Test. In the gain-of-function studies, no significant differences were observed in mitochondrial respiration (Fig. 4J). However, loss of NLRX1 in the $4T1^{KD}$ cells resulted in a significant shift in mitochondrial respiration, most evident in the basal respiration and maximal respiration (Fig. 4J). These trends were consistent under TNF and TGF-β conditions (Fig. 4K, 4L). We also observed 4-fold more spare respiratory capacity in $4T1^{KD}$ cells compared with the $4T1^{KD\text{-}CTL}$ cells (Fig. 4M). This coincided with approximately double the spare respiratory capacity in $4T1^{OE\text{-}CTL}$ cells compared with $4T1^{OE}$ cells, although this was not statistically significant ($p = 0.16$). The spare respiratory capacity phenotypes were consistent under TNF and TGF-β conditions (Fig. 4N, 4O). Taken together, these data show that the knockdown of NLRX1 alters several cancer hallmarks in the 4T1 cells, including decreasing proliferation, migration, and ROS production, and increasing cell death and respiratory capacity. Conversely, the overexpression of NLRX1 appears to reverse some of these same biological functions.

NLRX1 expressed in 4T1 cells promotes tumor growth and metastasis in vivo

We have demonstrated that NLRX1 functions as a tumor promoter when overexpressed in the 4T1 mammary tumor cells. We next sought to determine whether the increased aggressiveness observed in vitro translated to increased disease burden in vivo. We injected 1.2×10^6 cells (either $4T1^{OE}$, $4T1^{OE\text{-}CTL}$, $4T1^{KD}$, or $4T1^{KD\text{-}CTL}$) into a singular mammary fat pad of WT and *Nlrx1*$^{-/-}$ mice (Fig. 5A, 5F). Mice were monitored for morbidity and tumor growth throughout the study and euthanized on day 14 postinjection for tissue collection. Minimal differences in tumor growth were observed in any of the groups (Fig. 5B, 5G), but differences became more pronounced upon necropsy. In the mice engrafted with $4T1^{OE}$ tumors, we observed a doubling of final tumor volume compared with mice engrafted with $4T1^{OE\text{-}CTL}$ tumors in both WT and *Nlrx1*$^{-/-}$ mice (Fig. 5C). However, no differences in final tumor volume were observed in either WT or *Nlrx1*$^{-/-}$ mice engrafted with the knockdown tumors ($4T1^{KD}$) or their controls ($4T1^{KD\text{-}CTL}$) (Fig. 5H).

In addition to tumor growth, morbidity was monitored during the course of the study and quantified using a health scoring system (range of 0–4). By harvesting animals with smaller tumors at day 14, morbidity can be minimized (Fig. 5D, 5I). We observed a significant increase in clinical scores, indicating an increased severity in morbidity, in WT mice engrafted with $4T1^{KD\text{-}CTL}$ tumors compared with WT mice engrafted with $4T1^{KD}$ tumors on days 12–14 postinjection (Fig. 5I). Upon further investigation, we determined that the differences in morbidity were driven by tumor eschar. Tumor eschar is necrotic tissue that forms an ulcerating lesion around the center of the mammary tumor on the surface of the skin and can occur during the 4T1 model (39). Consistent with the increased health scores, WT mice engrafted with $4T1^{KD\text{-}CTL}$ tumors displayed more severe tumor eschar than those engrafted with $4T1^{KD}$ tumors (Fig. 5J).

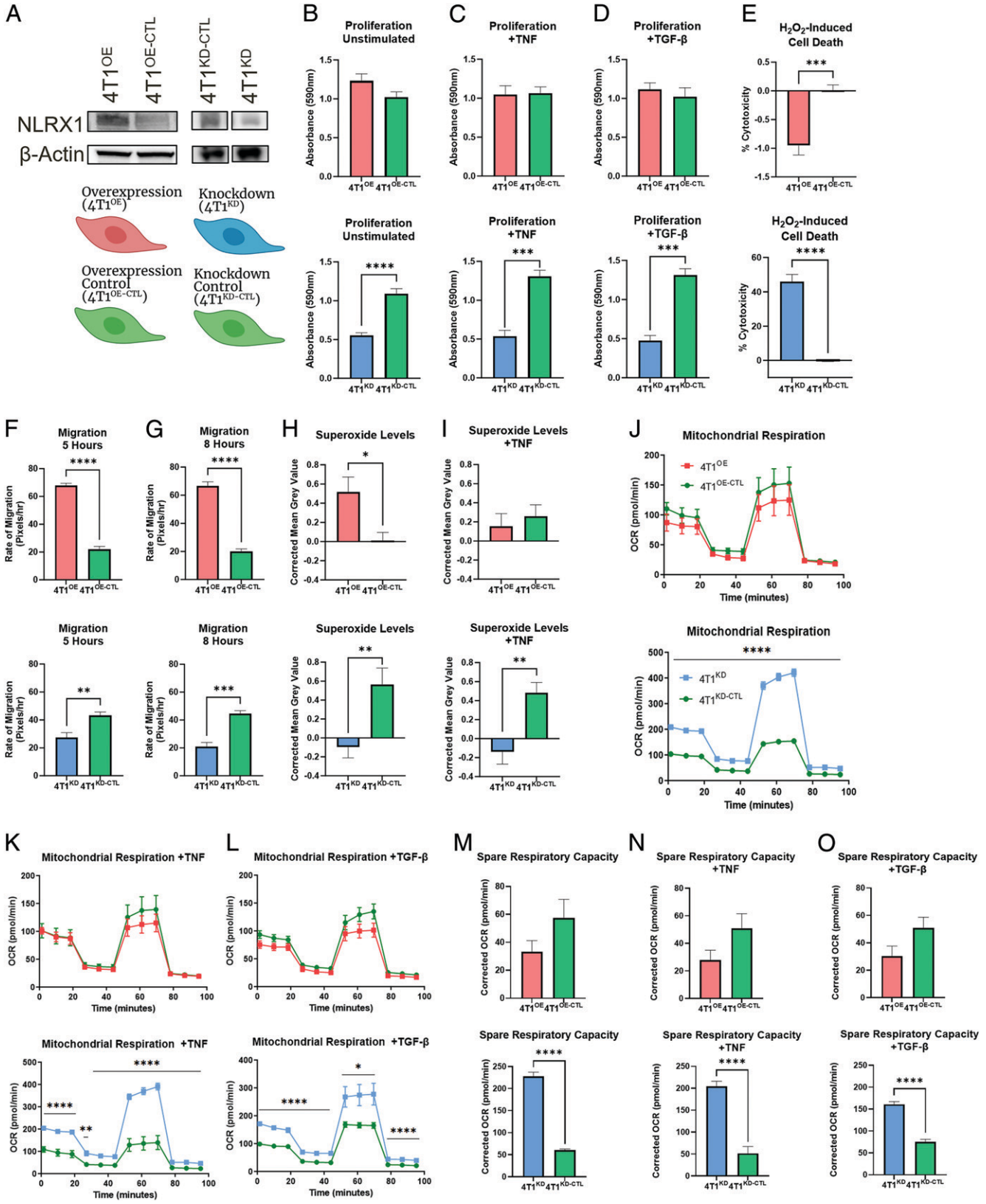

FIGURE 4. NLRX1 expressed in 4T1 cells enhances their aggressive properties in vitro. (**A**) Western blot verification of NLRX1 knockdown ($4T1^{KD}$) and overexpression ($4T1^{OE}$) in 4T1 cells with separate control cell lines ($4T1^{KD\text{-}CTL}$, $4T1^{OE\text{-}CTL}$) and schematic of generated cells and color scheme for data. (**B**–**O**) Differences between $4T1^{OE}$ cells versus $4T1^{OE\text{-}CTL}$ cells, and between $4T1^{KD}$ cells versus $4T1^{KD\text{-}CTL}$ cells for (B) proliferation in unstimulated conditions, (C) proliferation following TNF stimulation, (D) proliferation following TGF-β stimulation, (E) H_2O_2-induced cell death, (F) migration at 5 h, (G) migration at 8 h, (H) mitochondrial ROS (superoxide) levels in unstimulated conditions, (I) superoxide levels following TNF stimulation, (J) mitochondrial respiration in unstimulated conditions, (K) mitochondrial respiration following TNF stimulation, (L) mitochondrial respiration following TGF-β stimulation, (M) spare respiratory capacity in unstimulated conditions, (N) spare respiratory capacity following TNF stimulation, and *(Figure legend continues)*

This trend was also present in the *Nlrx1*$^{-/-}$ mice, but it was not statistically significant (Fig. 5I, Supplemental Fig. 4A). There were no differences in morbidity in either WT or *Nlrx1*$^{-/-}$ mice with 4T1^{OE} or 4T1$^{OE\text{-}CTL}$ tumors (Fig. 5D). Thus, although this phenotype could be an artifact of the knockdown construct or delivery method in the WT$^{KD\text{-}CTL}$ animals, the severity of tumor eschar in mice with 4T1$^{KD\text{-}CTL}$ tumors may suggest a role for NLRX1 in promoting this biological phenomenon.

Consistent with the increased migration observed in the in vitro studies (Fig. 4F, 4G), the metastatic burden was significantly increased in mice engrafted with 4T1^{OE} tumors compared with 4T1$^{OE\text{-}CTL}$ tumors in WT and *Nlrx1*$^{-/-}$ mice, with 4-fold ($\log_2$) and 3-fold ($\log_2$) increases, respectively (Fig. 5E). Consistent with the decreased migration observed in the in vitro studies (Fig. 4F, 4G), the metastatic burden was significantly decreased in WT mice engrafted with 4T1^{KD} tumors compared with those engrafted with 4T1$^{KD\text{-}CTL}$ tumors (Fig. 5K). In the *Nlrx1*$^{-/-}$ mice, we observed 3-fold less lung metastasis in mice engrafted with 4T1^{KD} tumors compared with those with 4T1$^{KD\text{-}CTL}$ tumors, but this was not statistically significant ($p = 0.16$) (Fig. 5K). Quantification of lung metastasis was acquired either through percent metastatic burden or a manual count of metastatic colonies, both of which have been previously described (39, 41).

Taking into consideration the results of the in vivo studies with the parental 4T1 cells (Fig. 1) and the in vitro cell line studies (Fig. 4), we predicted that *Nlrx1*$^{-/-}$ mice engrafted with 4T1^{OE} cells (*Nlrx1*$^{-/-}$ 4T1^{OE}) would have the most severe disease burden. To confirm this, we evaluated the tumor growth, morbidity, final tumor volume, and lung metastasis data to compare the results between all four comparisons in each study (Supplemental Fig. 4B–I). Indeed, the loss of the protective effects of NLRX1 in healthy host cells in *Nlrx1*$^{-/-}$ mice combined with the overexpression of NLRX1 in the 4T1^{OE} cells resulted in the highest metastatic burden that more than doubled the levels observed in the WT mice with the same 4T1^{OE} cells (Supplemental Fig. 4H). No additional significant differences were noted between WT and *Nlrx1*$^{-/-}$ mice engrafted with the same 4T1 cells (Supplemental Fig. 4B–I). Importantly, the in vivo studies with parental 4T1 cells were longer in duration than those with transduced 4T1 cells (24 versus 14 d). The shortened study duration of the in vivo studies with transduced 4T1 cells may have prevented robust differences between WT and *Nlrx1*$^{-/-}$ mice that we observed in the in vivo studies with parental 4T1 cells, especially considering that the differences in tumor growth with the parental 4T1 cells became more evident after day 14 (Fig. 1A). Taken together, the in vivo overexpression and knockdown studies revealed that NLRX1 augments 4T1 mammary tumor growth and metastasis when expressed in the 4T1 cancer cells, which is a reversal of NLRX1 function when expressed in the healthy host cells.

NLRX1 expressed in 4T1 cells augments lung metastasis through promoting EMT

To define the mechanisms responsible for the phenotypes observed during the in vivo studies utilizing the overexpression and knockdown 4T1 cells, we again used a transcriptomics approach. In this study, we focused our analysis on the NLRX1 overexpression tumors (4T1^{OE}) and their controls (4T1$^{OE\text{-}CTL}$) due to the in vivo phenotypes being more pronounced in the overexpression studies (Fig. 5). Through transcriptomics microarray analysis, we identified the top pathways impacted by NLRX1 as dictated by the number of DEGs (Fig. 6A). Pathways with enough DEGs to rank in the top 20 in at least two of the four comparisons were considered "top pathways." Pathways that overlap with pathways identified in the studies using unmodified 4T1 cells (Fig. 2A) were noted here with a star (Fig. 6A). Many of the top pathways were again important to EMT, including EGFR1 signaling, focal adhesion, PI3K-AKT-mTOR, MAPK, and TGF-β receptor signaling pathways (Fig. 6A). Interestingly, the regulation of these EMT-related pathways is more significant, as dictated by the TAC software's predictions, between 4T1^{OE} and 4T1$^{OE\text{-}CTL}$ tumors than between *Nlrx1*$^{-/-}$ and WT mice, suggesting that NLRX1 has a larger impact on EMT when expressed by 4T1 cells than by healthy host cells (Fig. 6A). We then identified the DEGs in the EMT-related pathways between 4T1^{OE} and 4T1$^{OE\text{-}CTL}$ tumors in *Nlrx1*$^{-/-}$ (Fig. 6B) and WT mice (Fig. 6C) and found the signature in 4T1^{OE} tumors to be consistent with the promotion of EMT (Fig. 6B, 6C). More specifically, we identified 27 DEGs in tumors from *Nlrx1*$^{-/-}$ mice and 13 DEGs in tumors from WT mice specifically related to EMT that were generally upregulated in the 4T1^{OE} tumors (Fig. 6D, 6E, Supplemental Fig. 4J) (42). Consistent with the increased disease burden when NLRX1 is overexpressed in the tumor and lacking in the host, there are more EMT-related DEGs in tumors from *Nlrx1*$^{-/-}$ mice compared with tumors in the WT animals (Fig. 6B–E). Again, this suggests that the aggressive characteristics fostered by NLRX1 in the 4T1 cells outweigh the protective characteristics fostered by NLRX1 in the host cells.

We then analyzed protein levels of the epithelial marker E-cadherin and found that 4T1^{OE} tumors express less E-cadherin than 4T1$^{OE\text{-}CTL}$ tumors do in WT and *Nlrx1*$^{-/-}$ mice (Fig. 6F, Supplemental Fig. 4K). This is consistent with in vitro and in vivo data that demonstrate overexpression of NLRX1 in 4T1 cells confers an advantage to the tumor and promotes EMT. Conversely, 4T1^{KD} tumors retained E-cadherin whereas 4T1$^{KD\text{-}CTL}$ tumors lost E-cadherin in both WT and *Nlrx1*$^{-/-}$ mice; however, this was only statistically significant in the *Nlrx1*$^{-/-}$ mice (Fig. 6F, Supplemental Fig. 4K). Again, this is consistent with our in vitro and in vivo data that indicate the loss of NLRX1 in 4T1 cells confers a loss of aggressiveness and decreased disease burden. The transcriptomics analysis predicted that NLRX1 in 4T1 cells likely promotes hallmarks of EMT through the upregulation of the genes encoding growth factors TGF-β3 and HB-EGF, c-Kit, VEGFR1, and Notch1/2 receptors, and promoting Smad, p38 MAPK, PI3K-AKT, MAPK/ERK, and β-catenin pathways (Fig. 6G). Taken together, these pathways converge on the transcription factors *Snail1* and *Tcf4* (Fig. 6G).

Discussion

Since its initial discovery and characterization, the signaling, function, and even cellular localization of NLRX1 have been heavily debated (10, 11, 16–18, 25, 27, 36, 37, 57). Beyond infectious disease studies, there is significant interest in better defining the role of NLRX1 in cancer (7). The current literature characterizes NLRX1 as both a tumor promoter and a tumor suppressor (20, 21, 23, 24, 27, 37, 38). These seemingly contradictory findings have added to NLRX1's intrigue and have resulted in general confusion in the field regarding its biological functions.

(O) spare respiratory capacity following TGF-β stimulation. All data were analyzed using a two-way unpaired *t* test except mitochondrial respiration, which was analyzed using multiple *t* tests (one per row). All data are shown as mean ± SEM. $n = 4$–15 for each cell type per study. All data are representative of at least one to two independent studies. *$p \leq 0.05$, **$p \leq 0.01$, ***$p \leq 0.001$, **** $p \leq 0.0001$.

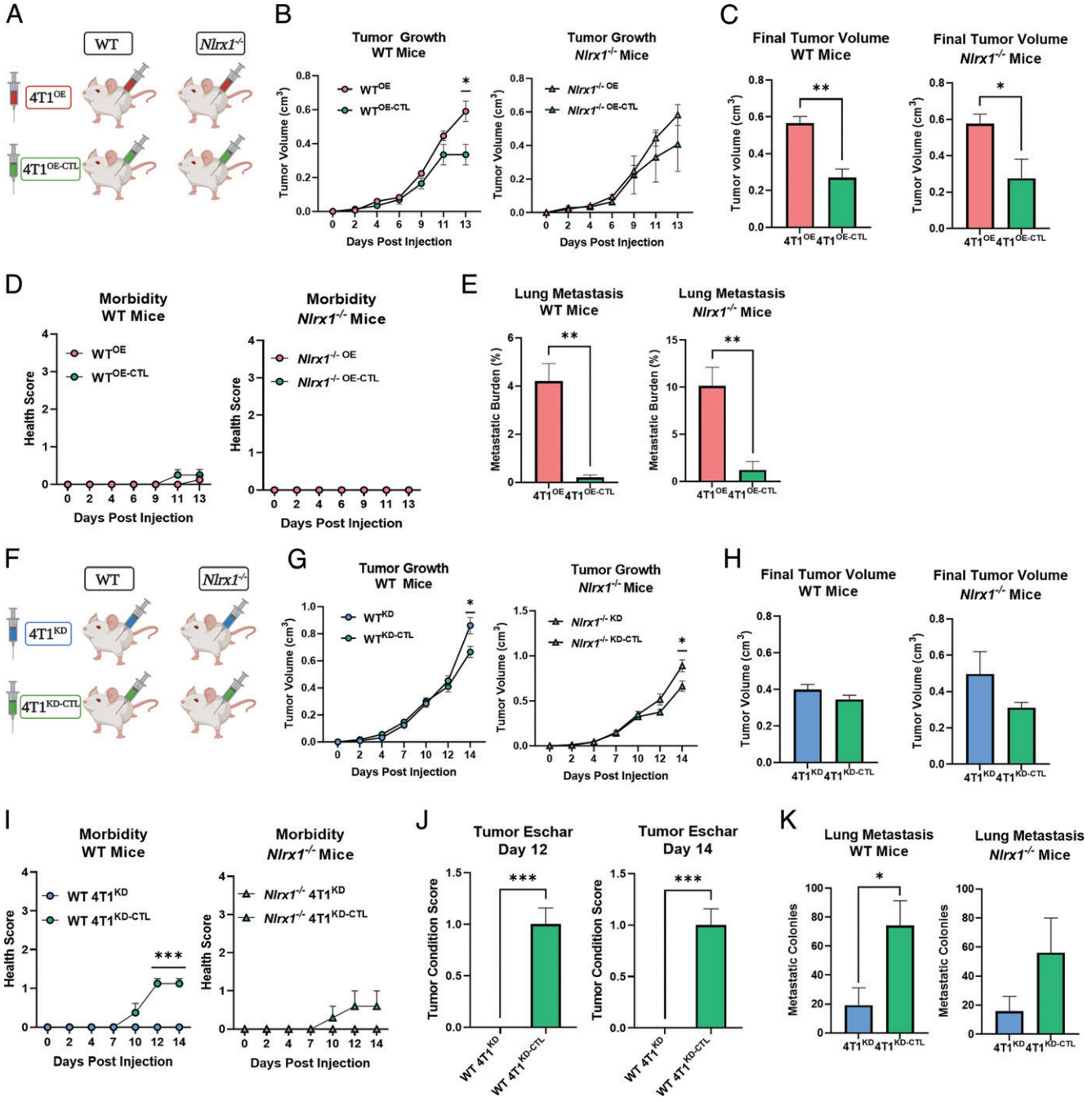

FIGURE 5. NLRX1 expressed in 4T1 cells promotes tumor growth and metastasis in vivo. (**A**) Study design for WT and *Nlrx1*$^{-/-}$ mice injected with either 4T1^{OE} or 4T1$^{OE\text{-}CTL}$ cells and color scheme for data. Data are representative of two independent experiments. (**B**–**E**) Differences between 4T1^{OE} tumors and 4T1$^{OE\text{-}CTL}$ tumors in WT and *Nlrx1*$^{-/-}$ mice in (B) tumor volume estimates based on two-dimensional measurements, (C) three-dimensional final tumor volume measurements, (D) morbidity, and (E) lung metastasis. (**F**) Study design for WT and *Nlrx1*$^{-/-}$ mice injected with either 4T1^{KD} or 4T1$^{KD\text{-}CTL}$ cells and color scheme for data. Data are representative of one independent experiment. (**G**–**K**) Differences between 4T1^{KD} and 4T1$^{KD\text{-}CTL}$ tumors in WT and *Nlrx1*$^{-/-}$ mice in (G) tumor volume estimates based on two-dimensional measurements, (H) three-dimensional final tumor volume measurements, (I) morbidity, (J) tumor eschar as determined by tumor condition score, and (K) lung metastasis. Final tumor volume, lung metastasis, and tumor eschar were analyzed using a two-way unpaired *t* test. Tumor growth and morbidity were analyzed using multiple *t* tests (one per row). Data are shown as mean ± SEM. $n = 3–5$ per group per study. See also Supplemental Fig. 4. $*p \leq 0.05$, $**p \leq 0.01$, $***p \leq 0.001$.

The lack of in vivo syngeneic tumor models and studies utilizing *Nlrx1*$^{-/-}$ mice have been limitations with prior studies, especially in breast cancer studies, which have focused on in vitro characterization in varying cell lines. In this study, we circumvented these prior limitations by using both loss-of-function and gain-of-function 4T1 cells and *Nlrx1*$^{-/-}$ mice fully backcrossed onto the BALB/cJ background for syngeneic mammary tumor studies using the same parental cell line. Our data demonstrate that NLRX1 functions differently depending on whether it is expressed in the host cells or in the 4T1 tumor cells. In the host cells, NLRX1 functions as a tumor suppressor where it limits tumor progression and metastasis. Conversely, in the 4T1 mammary tumor cells, NLRX1 functions as a tumor promoter that enhances malignant properties. Taken together, these data provide insight into some of the controversy and confusion associated with this NLR by revealing a dichotomy between NLRX1 functions based on cellular context. Previous work in other cancer models has

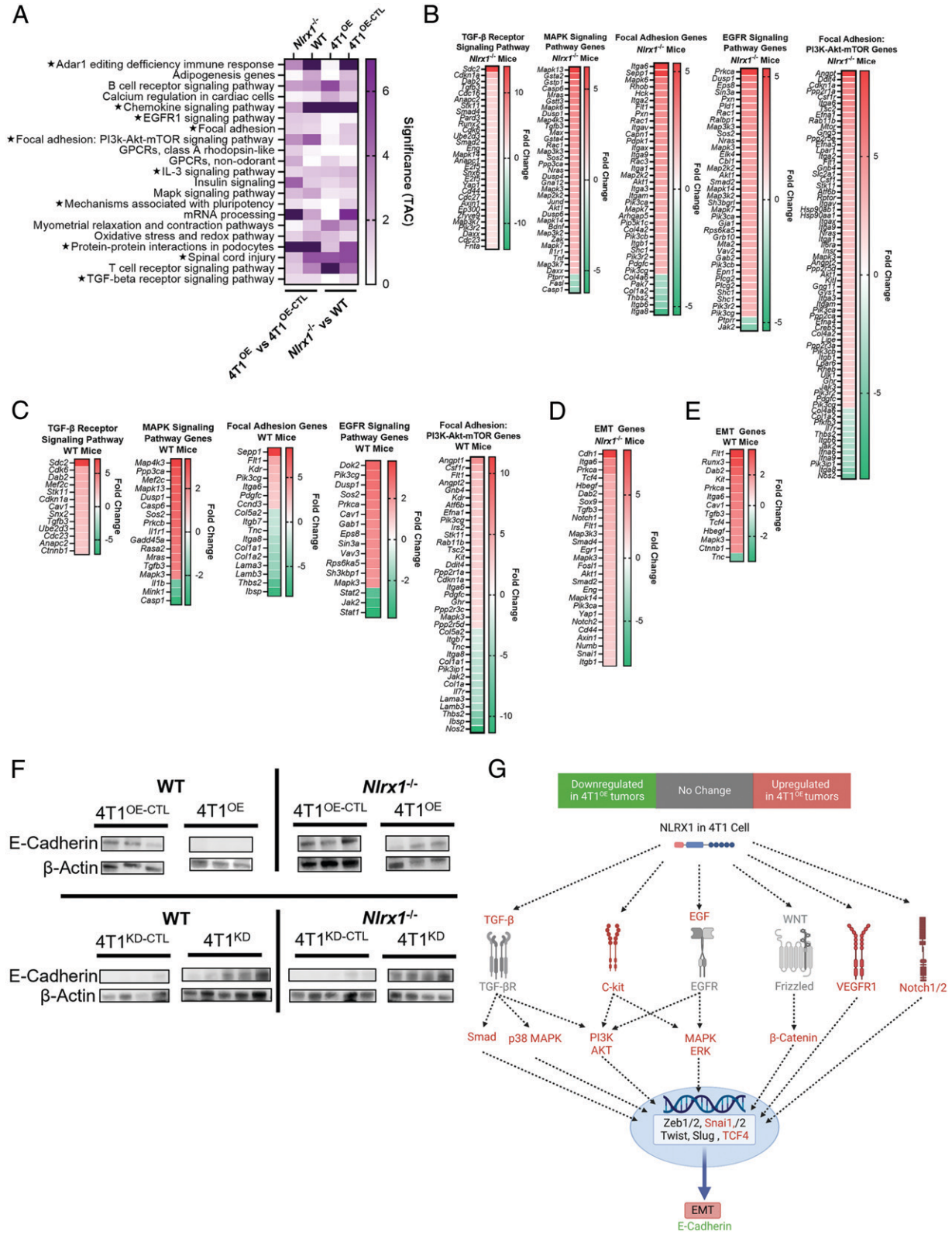

FIGURE 6. NLRX1 expressed in 4T1 cells augments lung metastasis through promoting epithelial–mesenchymal transition. (**A**) Twenty pathways were identified by the number of DEGs in the Transcriptomics Analysis Console (TAC) software in at least two of the four groups compared, listed here alphabetically as a heat map of TAC significance. (**B** and **C**) Heat maps of DEGs from epithelial–mesenchymal transition (EMT)–related pathways in TAC between $4T1^{OE}$ versus $4T1^{OE\text{-}CTL}$ tumors in (B) *Nlrx1*$^{-/-}$ mice and (C) WT mice. (**D** and **E**) Heat map of EMT-related DEGs between $4T1^{OE}$ versus $4T1^{OE\text{-}CTL}$ tumors in (D) *Nlrx1*$^{-/-}$ mice and (E) WT mice. (**F**) Western blot of E-cadherin from WT and *Nlrx1*$^{-/-}$ mice with either $4T1^{OE}$, $4T1^{OE\text{-}CTL}$, $4T1^{KD}$, or $4T1^{KD\text{-}CTL}$ tumors. (**G**) TAC analysis of transcriptomics data predicted multiple pathways upregulated by NLRX1 in 4T1 cells that converge to increase EMT. See also Supplemental Fig. 4.

shown that tumor-suppressive functions of NLRX1 in host cells stem from the nonhematopoietic compartment, although identifying which populations of healthy host cells provide the protective phenotypes in a mammary tumor model remains unexplored (20).

Our data revealed several overlapping pathways that were altered following the manipulation of NLRX1. Many of these pathways have previously been found to be regulated by NLRX1 in either infectious disease or cancer studies. For example, we demonstrate that NLRX1 in both healthy host cells and 4T1 tumor cells impacts EGFR signaling, which is consistent with prior studies in head and neck squamous cell carcinoma where NLRX1 appears to form a critical signaling hub that augments autophagy (61). However, we show that the upregulation or downregulation of EGFR signaling by NLRX1 is dependent on cellular context. Additionally, NLRX1 negatively regulated AKT, MAPK, and NF-κB signaling in a model of chemical-induced histiocytic sarcoma (23). This is consistent with colorectal cancer studies where NLRX1 was found to function as a tumor suppressor through inhibiting NF-κB, MAPK, STAT3, and IL-6 signaling, and *Nlrx1* deficiency on the $Apc^{min/+}$ background resulted in increased proliferation and expression of β-catenin (20). In general, our data are consistent with these prior findings that identify NLRX1 as a regulator of AKT, MAPK, ERK, IL-6, and β-catenin, although we demonstrate that the upregulation or downregulation of these overlapping pathways by NLRX1 is dependent on cellular context. Intriguingly, we did not observe significant dysregulation of NF-κB signaling in the tumors from any of our studies. It is possible that the inflammatory nature of the histiocytic sarcoma and colorectal cancer models were stronger inducers of NF-κB signaling compared with the relatively immunosuppressive nature of the 4T1 model (39). Although NF-κB signaling was not significant in the tumors, we did find an anti-inflammatory role for NLRX1 in the lung, where NLRX1 in host cells impeded characteristics of the metastatic niche. We also revealed a lesser-studied role for NLRX1 in the metastatic niche regarding ECM remodeling and immune cell recruitment, both of which are relatively undefined functions of NLRX1, especially in cancer (21, 30, 38, 49, 52).

Although our data reveal differences in function based on the cellular context, our studies converge on NLRX1 regulation of EMT as the mechanism underlying the phenotypes observed in our in vivo studies. Loss of E-cadherin during EMT has been observed in aggressive and invasive breast tumors and leads to the destabilization of adherens junctions, cancer cell survival, invasiveness, and metastasis (62–64). Additionally, increased MMP9 and TGF-β promote tumor progression and metastasis through regulating EMT (62, 63, 65). In the current study, we find that NLRX1 expression in healthy host cells retains E-cadherin levels and suppresses MMP9 and TGF-β levels in the tumor, conferring protection against EMT and metastasis. Conversely, we find that NLRX1 expression in the 4T1 mammary tumor cells decreases E-cadherin levels in the tumor and causes increased EMT and metastasis. Importantly, differences in protein levels were not always statistically significance due to the variability between individual mice and the plastic nature of EMT. However, the statistically insignificant differences in protein expression patterns were nonetheless notable, especially when taken into consideration alongside the gene expression data. Our transcriptomics and pathway analyses predict that the diametric regulation of EMT markers by NLRX1 in different cellular contexts is caused by regulation of *β-catenin*, *Snail1*, *Zeb2*, and *Tcf4*, which repress E-cadherin expression or are downregulated by E-cadherin (64, 66–68). Mechanistically, it is possible that NLRX1 directly regulates E-cadherin, MMP9, and TGF-β through the formation of multiprotein complexes similar to the so-called TRAFasomes that have been described for related NLRs (9).

Only one previous study has examined the role of NLRX1 in EMT (21). Using two different human cell lines, Hu et al. (21) explored NLRX1 in hepatocellular carcinoma by overexpressing NLRX1 in HCCLM3 cells and knocking down NLRX1 in Huh7 cells. The study found that NLRX1 overexpression increased E-cadherin expression and decreased N-cadherin, vimentin, Snail1, and Twist1 expression. Conversely, the knockdown of NLRX1 resulted in the opposite expression pattern, suggesting that NLRX1 suppresses EMT in both hepatocellular carcinoma cell lines. The authors concluded that NLRX1 in hepatocellular carcinoma cells suppresses EMT by inhibiting the PI3K-AKT pathway and subsequently downregulating Snail1 expression. These results counter what we find in the current study, where NLRX1 overexpression in 4T1 tumor cells decreases E-cadherin and NLRX1 knockdown retains E-cadherin. However, the importance of AKT signaling is consistent between both the hepatocellular carcinoma cell lines and our mammary tumor model. More work is certainly needed to further define the underlying mechanisms of this regulation in different types of cancer.

Beyond the tumor microenvironment and regulation of EMT, we also identified a role for NLRX1 in regulating ROS production and mitochondrial function in the 4T1 cells. In the mitochondrial electron transport chain, NLRX1 was previously found to interact with complex I and complex III to regulate ATP levels, and to interact with UQCRC2 of complex III to promote ROS production (27, 32). Specifically in MCF-7 human breast carcinoma cells, NLRX1 acts as a tumor suppressor through inhibiting the activity of the mitochondrial respiratory chain and generating TNF-induced superoxide (27). These MCF-7 results are the opposite of our findings in the current study in 4T1 cells and findings in MDA-MB-231 human TNBC cells that show NLRX1 serves as a tumor promoter when expressed in tumor cells (36). In MDA-MB-231 cells, the tumor-promoting phenotypes of NLRX1 were found to be a function of mitochondria–lysosomal crosstalk, and knockdown of NLRX1 increased ROS levels (36). However, our data show that the knockdown of NLRX1 reduces ROS levels in line with the increased spare respiratory capacity in $4T1^{KD}$ cells. Based on the high spare respiratory capacity in our $4T1^{KD}$ cells, there is a significant improvement for adapting and dealing with stress conditions, which would predict these cells to have lower ROS and superoxide production as they maximize respiratory rate, ATP synthesis, and ROS scavenging (60, 69, 70). In the current study, dysregulated mitochondrial function and increased superoxide levels are at least partially responsible for the tumor-promoting phenotypes of NLRX1 in 4T1 cells. Overall, our data warrant similar studies using additional syngeneic murine mammary tumor cell lines for in vivo studies to understand whether our observations are specific to 4T1 cells or whether these results are consistent across mammary tumor models, such as those with different hormone receptor statuses.

In conclusion, our data suggest that NLRX1 functions as a tumor promoter in the 4T1 mammary tumor cells, while simultaneously and conversely serving as a tumor suppressor in healthy host cells. These findings provide insight into the often-conflicting data generated in studies evaluating NLRX1, where function is likely specific to cell-type, stimuli, situational, and/or temporal factors. For NLRX1 in breast cancer, the dichotomy of effects observed in the tumor cells versus the healthy host cells is of critical importance for the design of future therapeutics. Our data would suggest that activating NLRX1 in healthy host cells or attenuating NLRX1 in cancer cells would be successful in attenuating the disease burden. However, this is cautionary, as any therapeutic that reverses this pattern would likely result in more aggressive disease. Although the mechanisms of NLRX1 are still not completely defined, this research has identified several biological functions that are significantly impacted by

NLRX1 in mammary tumors and their underlying mechanisms, thereby providing insights into the role of this enigmatic NLR family member in this deadly disease.

Acknowledgments

We thank Hannah Ivester and Dr. Brie Trusiano for support and teamwork, Dr. Thomas Cecere and the Cell Morphology Core at the Virginia Maryland College of Veterinary Medicine, the Metabolism Core at Virginia Tech, Melissa Makris and the Flow Cytometry Core at Virginia Tech, Bettina Heid for logistical support, and the Animal Care Staff and University Veterinarians at Virginia Tech. We also thank Dr. Jenny Ting of the University of North Carolina at Chapel Hill for the use of C57/BL6J *Nlrx1*$^{-/-}$ mice in our backcrossing methods. Summary figures were created with BioRender.com.

Disclosures

David A. Brown is employed by Stealth BioTherapeutics, a biotechnology company that is developing potential therapeutics for mitochondrial diseases. The other authors have no financial conflicts of interest.

References

1. Siegel, R. L., K. D. Miller, N. S. Wagle, and A. Jemal. 2023. Cancer statistics, 2023. *CA Cancer J. Clin.* 73: 17–48.
2. Giaquinto, A. N., H. Sung, K. D. Miller, J. L. Kramer, L. A. Newman, A. Minihan, A. Jemal, and R. L. Siegel. 2022. Breast cancer statistics, 2022. *CA Cancer J. Clin.* 72: 524–541.
3. Man, S. M., and B. J. Jenkins. 2022. Context-dependent functions of pattern recognition receptors in cancer. *Nat. Rev. Cancer* 22: 397–413.
4. Kayagaki, N., S. Warming, M. Lamkanfi, L. Vande Walle, S. Louie, J. Dong, K. Newton, Y. Qu, J. Liu, S. Heldens, et al. 2011. Non-canonical inflammasome activation targets caspase-11. *Nature* 479: 117–121.
5. Martinon, F., K. Burns, and J. Tschopp. 2002. The inflammasome: a molecular platform triggering activation of inflammatory caspases and processing of proIL-beta. *Mol. Cell* 10: 417–426.
6. Coutermarsh-Ott, S., K. Eden, and I. C. Allen. 2016. Beyond the inflammasome: regulatory NOD-like receptor modulation of the host immune response following virus exposure. *J. Gen. Virol.* 97: 825–838.
7. Allen, I. C. 2014. Non-inflammasome forming NLRs in inflammation and tumorigenesis. *Front. Immunol.* 22: 169.
8. Xia, X., J. Cui, H. Y. Wang, L. Zhu, S. Matsueda, Q. Wang, X. Yang, J. Hong, Z. Songyang, Z. J. Chen, and R. F. Wang. 2011. NLRX1 negatively regulates TLR-induced NF-κB signaling by targeting TRAF6 and IKK. *Immunity* 34: 843–853.
9. Schneider, M., A. G. Zimmermann, R. A. Roberts, L. Zhang, K. V. Swanson, H. Wen, B. K. Davis, I. C. Allen, E. K. Holl, Z. Ye, et al. 2012. The innate immune sensor NLRC3 attenuates Toll-like receptor signaling via modification of the signaling adaptor TRAF6 and transcription factor NF-κB. *Nat. Immunol.* 13: 823–831.
10. Allen, I. C., C. B. Moore, M. Schneider, Y. Lei, B. K. Davis, M. A. Scull, D. Gris, K. E. Roney, A. G. Zimmermann, J. B. Bowzard, et al. 2011. NLRX1 protein attenuates inflammatory responses to infection by interfering with the RIG-I-MAVS and TRAF6-NF-κB signaling pathways. *Immunity* 34: 854–865.
11. Moore, C. B., D. T. Bergstralh, J. A. Duncan, Y. Lei, T. E. Morrison, A. G. Zimmermann, M. A. Accavitti-Loper, V. J. Madden, L. Sun, Z. Ye, et al. 2008. NLRX1 is a regulator of mitochondrial antiviral immunity. *Nature* 451: 573–577.
12. Chen, S.-T., L. Chen, D. S.-C. Lin, S.-Y. Chen, Y.-P. Tsao, H. Guo, F.-J. Li, W.-T. Tseng, J. W. Tam, C.-W. Chao, et al. 2019. NLRP12 regulates anti-viral RIG-I activation via interaction with TRIM25. *Cell Host Microbe* 25: 602–616.e7.
13. Allen, I. C., J. D. Lich, J. C. Arthur, C. M. Jania, R. A. Roberts, J. B. Callaway, S. L. Tilley, and J. P.-Y. Ting. 2012. Characterization of NLRP12 during the development of allergic airway disease in mice. *PLoS One* 7: e30612.
14. Zhang, L., J. Mo, K. V. Swanson, H. Wen, A. Petrucelli, S. M. Gregory, Z. Zhang, M. Schneider, Y. Jiang, K. A. Fitzgerald, et al. 2014. NLRC3, a member of the NLR family of proteins, is a negative regulator of innate immune signaling induced by the DNA sensor STING. *Immunity* 40: 329–341.
15. Tattoli, I., L. H. Travassos, L. A. Carneiro, J. G. Magalhaes, and S. E. Girardin. 2007. The Nodosome: Nod1 and Nod2 control bacterial infections and inflammation. *Semin. Immunopathol.* 29: 289–301.
16. Nagai-Singer, M. A., H. A. Morrison, and I. C. Allen. 2019. NLRX1 is a multifaceted and enigmatic regulator of immune system function. *Front. Immunol.* 10: 2419.
17. Pickering, R. J., and L. M. Booty. 2021. NLR in eXile: emerging roles of NLRX1 in immunity and human disease. *Immunology* 162: 268–280.
18. Qin, Y., B. Xue, C. Liu, X. Wang, R. Tian, Q. Xie, M. Guo, G. Li, D. Yang, and H. Zhu. 2017. NLRX1 mediates MAVS degradation to attenuate the hepatitis C virus-induced innate immune response through PCBP2. *J. Virol.* 91: e01264-17.
19. Jiao, Q., W. Xu, X. Guo, H. Liu, B. Liao, X. Zhu, C. Chen, F. Yang, L. Wu, C. Xie, and L. Peng. 2021. NLRX1 can counteract innate immune response induced by an external stimulus favoring HBV infection by competitive inhibition of MAVS-RLRs signaling in HepG2-NTCP cells. *Sci. Prog.* 104: 368504211058036.
20. Koblansky, A. A., A. D. Truax, R. Liu, S. A. Montgomery, S. Ding, J. E. Wilson, W. J. Brickey, M. Mühlbauer, R.-M. T. McFadden, P. Hu, et al. 2016. The innate immune receptor NLRX1 functions as a tumor suppressor by reducing colon tumorigenesis and key tumor-promoting signals. *Cell Rep.* 14: 2562–2575.
21. Hu, B., G.-Y. Ding, P.-Y. Fu, X.-D. Zhu, Y. Ji, G.-M. Shi, Y.-H. Shen, J.-B. Cai, Z. Yang, J. Zhou, et al. 2018. NOD-like receptor X1 functions as a tumor suppressor by inhibiting epithelial-mesenchymal transition and inducing aging in hepatocellular carcinoma cells. *J. Hematol. Oncol.* 11: 28.
22. Zhang, H., Y. Xiao, R. Nederlof, D. Bakker, P. Zhang, S. E. Girardin, M. W. Hollmann, N. C. Weber, S. M. Houten, M. van Weeghel, et al. 2020. NLRX1 deletion increases ischemia-reperfusion damage and activates glucose metabolism in mouse heart. *Front. Immunol.* 11: 591815.
23. Coutermarsh-Ott, S., A. Simmons, V. Capria, T. LeRoith, J. E. Wilson, B. Heid, C. W. Philipson, Q. Qin, R. Hontecillas-Magarzo, J. Bassaganya-Riera, et al. 2016. NLRX1 suppresses tumorigenesis and attenuates histiocytic sarcoma through the negative regulation of NF-κB signaling. *Oncotarget* 7: 33096–33110.
24. Tattoli, I., S. A. Killackey, E. G. Foerster, R. Molinaro, C. Maisonneuve, M. A. Rahman, S. Winer, D. A. Winer, C. J. Streutker, D. J. Philpott, and S. E. Girardin. 2016. NLRX1 acts as an epithelial-intrinsic tumor suppressor through the modulation of TNF-mediated proliferation. *Cell Rep.* 14: 2576–2586.
25. Tattoli, I., L. A. Carneiro, M. Jéhanno, J. G. Magalhaes, Y. Shu, D. J. Philpott, D. Arnoult, and S. E. Girardin. 2008. NLRX1 is a mitochondrial NOD-like receptor that amplifies NF-κB and JNK pathways by inducing reactive oxygen species production. *EMBO Rep.* 9: 293–300.
26. Yin, H., G. Sun, Q. Yang, C. Chen, Q. Qi, H. Wang, and J. Li. 2017. NLRX1 accelerates cisplatin-induced ototoxity in HEI-OC1 cells via promoting generation of ROS and activation of JNK signaling pathway. *Sci. Rep.* 7: 44311.
27. Singh, K. A., A. Poteryakhina, K. Zheltukhin, P. Bhatelia, L. Prajapati, D. Sripada, R. Tomar, A. K. Singh, P. M. Singh, R. Chumakov, and R. Singh. 2015. NLRX1 acts as tumor suppressor by regulating TNF-α induced apoptosis and metabolism in cancer cells. *Biochim. Biophys. Acta* 1853: 1073–1086.
28. Stokman, G., L. Kors, P. J. Bakker, E. Rampanelli, N. Claessen, G. J. D. Teske, L. Butter, H. van Andel, M. A. van den Bergh Weerman, P. W. B. Larsen, et al. 2017. NLRX1 dampens oxidative stress and apoptosis in tissue injury via control of mitochondrial activity. *J. Exp. Med.* 214: 2405–2420.
29. Leber, A., R. Hontecillas, N. Tubau-Juni, V. Zoccoli-Rodriguez, V. Abedi, and J. Bassaganya-Riera. 2018. NLRX1 modulates immunometabolic mechanisms controlling the host-gut microbiota interactions during inflammatory bowel disease. *Front. Immunol.* 9: 363.
30. Leber, A., R. Hontecillas, N. Tubau-Juni, V. Zoccoli-Rodriguez, M. Hulver, R. McMillan, K. Eden, I. C. Allen, and J. Bassaganya-Riera. 2017. NLRX1 regulates effector and metabolic functions of $CD4^+$ T cells. *J. Immunol.* 198: 2260–2268.
31. Huang, J.-H., C.-Y. Liu, S.-Y. Wu, W.-Y. Chen, T.-H. Chang, H.-W. Kan, S.-T. Hsieh, J. P.-Y. Ting, and B. A. Wu-Hsieh. 2018. NLRX1 facilitates *Histoplasma capsulatum*-induced LC3-associated phagocytosis for cytokine production in macrophages. *Front. Immunol.* 9: 2761.
32. Arnoult, D., F. Soares, I. Tattoli, C. Castanier, D. J. Philpott, and S. E. Girardin. 2009. An N-terminal addressing sequence targets NLRX1 to the mitochondrial matrix. *J. Cell Sci.* 122: 3161–3168.
33. Lei, Y., H. Wen, and J. P.-Y. Ting. 2013. The NLR protein, NLRX1, and its partner, TUFM, reduce type I interferon, and enhance autophagy. *Autophagy* 9: 432–433.
34. Li, S., Y. Zhou, X. Gu, X. Zhang, and Z. Jia. 2021. NLRX1/FUNDC1/NIPSNAP1-2 axis regulates mitophagy and alleviates intestinal ischaemia/reperfusion injury. *Cell Prolif.* 54: e12986.
35. Zhang, Y., Y. Yao, X. Qiu, G. Wang, Z. Hu, S. Chen, Z. Wu, N. Yuan, H. Gao, J. Wang, et al. 2019. *Listeria* hijacks host mitophagy through a novel mitophagy receptor to evade killing. *Nat. Immunol.* 20: 433–446.
36. Singh, K., M. Roy, P. Prajapati, A. Lipatova, L. Sripada, D. Gohel, A. Singh, M. Mane, M. M. Godbole, P. M. Chumakov, and R. Singh. 2019. NLRX1 regulates TNF-α-induced mitochondria-lysosomal crosstalk to maintain the invasive and metastatic potential of breast cancer cells. *Biochim. Biophys. Acta Mol. Basis Dis.* 1865: 1460–1476.
37. Soares, F., I. Tattoli, M. A. Rahman, S. J. Robertson, A. Belcheva, D. Liu, C. Streutker, S. Winer, D. A. Winer, A. Martin, et al. 2014. The mitochondrial protein NLRX1 controls the balance between extrinsic and intrinsic apoptosis. *J. Biol. Chem.* 289: 19317–19330.
38. Luo, X., C. R. Donnelly, W. Gong, B. R. Heath, Y. Hao, L. A. Donnelly, T. Moghbeli, Y. S. Tan, X. Lin, E. Bellile, et al. 2020. HPV16 drives cancer immune escape via NLRX1-mediated degradation of STING. *J. Clin. Invest.* 130: 1635–1652.
39. Pulaski, B. A., and S. Ostrand-Rosenberg. 2000. Mouse 4T1 breast tumor model. *Curr. Protoc. Immunol.* Chapter 20: Unit 20.2.
40. Tomayko, M. M., and C. P. Reynolds. 1989. Determination of subcutaneous tumor size in athymic (nude) mice. *Cancer Chemother. Pharmacol.* 24: 148–154.
41. Nagai-Singer, M. A., A. Hendricks-Wenger, R. M. Brock, H. A. Morrison, J. D. Tupik, S. Coutermarsh-Ott, and I. C. Allen. 2020. Using computer-based image analysis to improve quantification of lung metastasis in the 4T1 breast cancer model. *J. Vis. Exp.* 164: e61805.
42. Zhao, M., L. Kong, Y. Liu, and H. Qu. 2015. dbEMT: an epithelial-mesenchymal transition associated gene resource. *Sci. Rep.* 5: 11459.
43. Onder, T. T., P. B. Gupta, S. A. Mani, J. Yang, E. S. Lander, and R. A. Weinberg. 2008. Loss of E-cadherin promotes metastasis via multiple downstream transcriptional pathways. *Cancer Res.* 68: 3645–3654.

44. Xu, J., S. Lamouille, and R. Derynck. 2009. TGF-β-induced epithelial to mesenchymal transition. *Cell Res.* 19: 156–172.
45. Wang, G., D. Xu, Z. Zhang, X. Li, J. Shi, J. Sun, H.-Z. Liu, X. Li, M. Zhou, and T. Zheng. 2021. The pan-cancer landscape of crosstalk between epithelial-mesenchymal transition and immune evasion relevant to prognosis and immunotherapy response. *NPJ Precis. Oncol.* 5: 56.
46. Taki, M., K. Abiko, M. Ukita, R. Murakami, K. Yamanoi, K. Yamaguchi, J. Hamanishi, T. Baba, N. Matsumura, and M. Mandai. 2021. Tumor immune microenvironment during epithelial-mesenchymal transition. *Clin. Cancer Res.* 27: 4669–4679.
47. Grisaru-Tal, S., M. Itan, A. D. Klion, and A. Munitz. 2020. A new dawn for eosinophils in the tumour microenvironment. *Nat. Rev. Cancer* 20: 594–607.
48. Fulkerson, P. C., H. Zhu, D. A. Williams, N. Zimmermann, and M. E. Rothenberg. 2005. CXCL9 inhibits eosinophil responses by a CCR3- and Rac2-dependent mechanism. *Blood* 106: 436–443.
49. Kastelberg, B., N. Tubau-Juni, T. Ayubi, A. Leung, A. Leber, R. Hontecillas, J. Bassaganya-Riera, and S. D. Kale. 2020. NLRX1 is a key regulator of immune signaling during invasive pulmonary aspergillosis. *PLoS Pathog.* 16: e1008854.
50. Zhang, C., Z. Li, L. Xu, X. Che, T. Wen, Y. Fan, C. Li, S. Wang, Y. Cheng, X. Wang, et al. 2018. CXCL9/10/11, a regulator of PD-L1 expression in gastric cancer. *BMC Cancer* 18: 462.
51. Jinesh, G. G., and A. S. Brohl. 2022. Classical epithelial-mesenchymal transition (EMT) and alternative cell death process-driven blebbishield metastatic-witch (BMW) pathways to cancer metastasis. *Signal Transduct. Target. Ther.* 7: 296.
52. Xu, H., L. Ji, C. Yu, Q. Chen, Q. Ge, and Y. Lu. 2020. MiR-423-5p regulates cells apoptosis and extracellular matrix degradation via nucleotide-binding, leucine-rich repeat containing X1 (NLRX1) in interleukin 1 beta (IL-1β)-induced human nucleus pulposus cells. *Med. Sci. Monit.* 26: e922497.
53. Sceneay, J., B. S. Parker, M. J. Smyth, and A. Möller. 2013. Hypoxia-driven immunosuppression contributes to the pre-metastatic niche. *OncoImmunology* 2: e22355.
54. Liu, Y., and X. Cao. 2016. Characteristics and significance of the pre-metastatic niche. *Cancer Cell* 30: 668–681.
55. Human Protein Atlas. Tissue expression of NLRX1—Summary. https://www.proteinatlas.org/ENSG00000160703-NLRX1/tissue. Accessed: August 3, 2023.
56. Uhlén, M., L. Fagerberg, B. M. Hallström, C. Lindskog, P. Oksvold, A. Mardinoglu, Å. Sivertsson, C. Kampf, E. Sjöstedt, A. Asplund, et al. 2015. Tissue-based map of the human proteome. *Science* 347: 1260419.
57. Soares, F., I. Tattoli, M. E. Wortzman, D. Arnoult, D. J. Philpott, and S. E. Girardin. 2013. NLRX1 does not inhibit MAVS-dependent antiviral signalling. *Innate Immun.* 19: 438–448.
58. Abdul-Sater, A. A., N. Saïd-Sadier, V. M. Lam, B. Singh, M. A. Pettengill, F. Soares, I. Tattoli, S. Lipinski, S. E. Girardin, P. Rosenstiel, and D. M. Ojcius. 2010. Enhancement of reactive oxygen species production and chlamydial infection by the mitochondrial Nod-like family member NLRX1. *J. Biol. Chem.* 285: 41637–41645.
59. Unger, B. L., S. Ganesan, A. T. Comstock, A. N. Faris, M. B. Hershenson, and U. S. Sajjan. 2014. Nod-like receptor X-1 is required for rhinovirus-induced barrier dysfunction in airway epithelial cells. *J. Virol.* 88: 3705–3718.
60. Aggarwal, V., H. S. Tuli, A. Varol, F. Thakral, M. B. Yerer, K. Sak, M. Varol, A. Jain, M. A. Khan, and G. Sethi. 2019. Role of reactive oxygen species in cancer progression: molecular mechanisms and recent advancements. *Biomolecules* 9: 735.
61. Lei, Y., B. A. Kansy, J. Li, L. Cong, Y. Liu, S. Trivedi, H. Wen, J. P.-Y. Ting, H. Ouyang, and R. L. Ferris. 2016. EGFR-targeted mAb therapy modulates autophagy in head and neck squamous cell carcinoma through NLRX1-TUFM protein complex. *Oncogene* 35: 4698–4707.
62. Hao, Y., D. Baker, and P. Ten Dijke. 2019. TGF-β-mediated epithelial-mesenchymal transition and cancer metastasis. *Int. J. Mol. Sci.* 20: 2767.
63. Dongre, A., and R. A. Weinberg. 2019. New insights into the mechanisms of epithelial-mesenchymal transition and implications for cancer. *Nat. Rev. Mol. Cell Biol.* 20: 69–84.
64. Wong, T.-S., W. Gao, and J. Y.-W. Chan. 2014. Transcription regulation of E-cadherin by zinc finger E-box binding homeobox proteins in solid tumors. *BioMed Res. Int.* 2014: 921564.
65. Owyong, M., J. Chou, R. J. van den Bijgaart, N. Kong, G. Efe, C. Maynard, D. Talmi-Frank, I. Solomonov, C. Koopman, E. Hadler-Olsen, et al. 2019. MMP9 modulates the metastatic cascade and immune landscape for breast cancer anti-metastatic therapy. *Life Sci. Alliance* 2: e201800226.
66. Conacci-Sorrell, M., I. Simcha, T. Ben-Yedidia, J. Blechman, P. Savagner, and A. Ben-Ze'ev. 2003. Autoregulation of E-cadherin expression by cadherin-cadherin interactions: the roles of β-catenin signaling, Slug, and MAPK. *J. Cell Biol.* 163: 847–857.
67. Peiró, S., M. Escrivà, I. Puig, M. J. Barberà, N. Dave, N. Herranz, M. J. Larriba, M. Takkunen, C. Francí, A. Muñoz, et al. 2006. Snail1 transcriptional repressor binds to its own promoter and controls its expression. *Nucleic Acids Res.* 34: 2077–2084.
68. Wang, Q., Z.-X. Sun, H. Allgayer, and H.-S. Yang. 2010. Downregulation of E-cadherin is an essential event in activating β-catenin/Tcf-dependent transcription and expression of its target genes in Pdcd4 knockdown cells. *Oncogene* 29: 128–138.
69. Marchetti, P., Q. Fovez, N. Germain, R. Khamari, and J. Kluza. 2020. Mitochondrial spare respiratory capacity: mechanisms, regulation, and significance in non-transformed and cancer cells. *FASEB J.* 34: 13106–13124.
70. Cortassa, S., B. O'Rourke, and M. A. Aon. 2014. Redox-optimized ROS balance and the relationship between mitochondrial respiration and ROS. *Biochim. Biophys. Acta* 1837: 287–295.